NEW CHEMICAL AEROSOL CHARACTERIZATION METHODS-EXAMPLES USING AGRICULTURAL AND URBAN AIRBORNE PARTICULATE MATTER

A Thesis

by

LIJUN ZHOU

Submitted to the Office of Graduate Studies of
Texas A&M University
in partial fulfillment of the requirements for the degree of

MASTER OF SCIENCE

August 2010

Major Subject: Atmospheric Sciences

NEW CHEMICAL AEROSOL CHARACTERIZATION METHODS-EXAMPLES USING AGRICULTURAL AND URBAN AIRBORNE PARTICULATE MATTER

A Thesis

by

LIJUN ZHOU

Submitted to the Office of Graduate Studies of
Texas A&M University
in partial fulfillment of the requirements for the degree of

MASTER OF SCIENCE

Approved by:

Chair of Committee, Gunnar W. Schade
Committee Members, Sarah D. Brooks
Don Collins
William H. Marlow
Head of Department, Kenneth P. Bowman

August 2010

Major Subject: Atmospheric Sciences

ABSTRACT

New Chemical Aerosol Characterization Methods- Examples Using Agricultural and Urban Airborne Particulate Matter.

(August 2010)

Lijun Zhou, B.A., Qingdao University;

M.S. Peking University

Chair of Advisory Committee: Dr. Gunnar W. Schade

This study explored different chemical characterization methods of agricultural and urban airborne particulate matter. Three different field campaigns are discussed. For the agricultural aerosols, measurement of the chemical composition of size-resolved agricultural aerosols collected from a ground site at the nominally downwind and upwind edge of a feedlot in West Texas were reported. High volume cascade impactor samplers were used for the collection of the particles, and two major analytical methods were applied to characterize different components of the aerosols, ion chromatography (IC) was used to measure ionic composition with the main targets being ammonium (NH_4^+), nitrate (NO_3^-), and sulfate (SO_4^{2-}), direct thermal desorption gas chromatography-mass spectrometry/flame ionization detection (GC-MS/FID) methodology was used to identify and quantify organic compounds in the aerosol particles.

For the urban aerosols, I report the measurement of mass, and the chemical composition of size-resolved aerosols collected from two different locations in Houston, analyzed by the thermal desorption GC-MS/FID method. The investigation of single particle composition using RM is reported as well: RM and chemical mapping techniques have been applied for the qualitative analysis of components in the samples of air particulate matter collected in downtown Houston.

DEDICATION

This dissertation is dedicated to my parents and husband for their continued support and encouragement throughout my education.

ACKNOWLEDGMENTS

I would like to thank my advisor, Dr. Gunnar Shade, for his insightful advice and patient encouragement toward completing my project. I have learned a lot of things from him especially to think individually. I appreciate his patience for me.

I am thankful to my committee member, Dr Sarah Brooks, who give me the opportunity to do Raman research, and motivated me to do what I would like. The same goes to my thesis committee members, Dr. Don Collins, Dr. William Marlow, and everybody who I have worked with.

TABLE OF CONTENTS

LIST OF TABLES

Page

LIST OF FIGURES

Page

CHAPTER I

INTRODUCTION

Increases in the size and number of concentrated animal feeding operations (CAFOs) have lead to an increase in public concern regarding the emission of atmospheric pollutants, including particulate matter (PM) and odor emissions. PM emissions impact atmospheric visibility directly, can indirectly affect the global radiation balance, and can be detrimental to human health. In addition, particles can affect cloud formation by causing changes in condensation nuclei. Large particles, commonly called dust, are usually associated with natural sources, such as wind-blown soil particles, and can be both a nuisance and health concern. Agricultural, fugitive dust is a significant source of local air pollution in the semi-arid southern Great Plains. The generation and emission of aerosol particles from animal feeding operations have long been known to affect local air quality, animal and human health (Rule et al., 2005; Schicker et al., 2009). It is also connected to direct environmental impacts on the surrounding environment, such as from odorous volatile or semi-volatile compounds transported with the agricultural particles (Miller et al., 2001; Merchant et al., 2005). Therefore, these agricultural aerosols must be considered in assessments of the impacts of aerosols on visibility, climate forcing and human health.

This thesis follows the style of *Geophysical Research Letters*.

Gaseous emissions from agriculture have been known as a significant regional, national, and global source of methane, ammonia, nitrogen oxides and nitrous oxide (NRC 2003; Hiranuma et al., 2010). These trace gas emissions are often associated with emissions from cattle feeding operations, such as open air animal feeding facilities (Parker et al., 2005). Daily formation and emission of trace gases through agricultural activities are issues of concern to the public and the government. However, accurate estimation of air emissions from Animal Feeding Operations (AFOs) is complicated by various factors, including the kinds and number of animals involved, their diets and housing, the management of their manure, and climate and weather conditions. State and federal regulators try to assess the impacts of agricultural production on air quality (Sweeten et al., 1998). However, accurate data for a number of regulated pollutants is lacking, and more measurements of agricultural aerosols are needed.

A better understanding of the chemical composition of PM is also necessary for a complete understanding of PM emissions and impacts (Takahama et al., 2007; Moffet et al., 2009). A number of studies have shown that the chemical composition of aerosols plays an important role in changing its physical properties, such as particle size and hygroscopicity (Brooks et al., 2002, 2004; Chan and Chan, 2003; Gysel et al., 2004).

Ammonia is arguably the most important trace gas emitted from animal feeding operations. After its emission, ammonia is normally converted into particle-phase ammonium in the atmosphere within several days. Under typical atmospheric conditions, conversion of ammonia to the particle phase is likely to happen by the reactions between ammonia and gas phase inorganic compounds, such as sulfuric acid or nitric acid, to form ammonium sulfate and ammonium nitrate, respectively (Kim and Seinfeld, 1996). Field measurements of ammonia at agricultural sites, however, especially at open air AFOs, representing a large fraction of the total animal population, are still limited. In fact, only a few studies have been conducted at feedlots representative of the large facilities that are often found in the southwest United States (Faulkner et al., 2008; Todd et al., 2008). One study was conducted by Koziel and coworkers (2004) at a large open air facility in the Texas Panhandle referred to as Feedlot C, where around 45,000 head of

cattle are housed on one square mile. Hourly averaged concentrations of NH_3 of ~700 ppbv were measured with a large standard deviation. Part of our work includes the measurement of ammonium in the particulate matter at the studied field site, and will be described below. Similar to ammonium, AFOs are also known to emit volatile fatty acids (VFAs) (Ngwabie et al., 2007); the latter can adsorb rapidly to the ambient aerosol depending on meteorological conditions and upwind ambient aerosol mass and composition. Results for identified VFAs will be presented as well.

Recently, several studies have introduced direct thermal desorption with subsequent gas chromatographic separation for the determination of organic compounds in atmospheric aerosols (Ho et al., 2004; Welthagen et al., 2003; Kotianová et al., 2004; Goldstein et al., 2008; Ding et al., 2009). Ho et al. (2004) provided an approach for the analysis of aerosol alkanes and polycyclic aromatic hydrocarbons (PAHs) instead of the traditional solvent extraction method (Sin, D.W et al 2002). In their approach, small strips of aerosol-laden filter materials were packed into a GC split/splitless injector liner. Alkanes and PAHs on the filter are thermally desorbed in the injection port and focused onto the head of a GC column for subsequent separation and detection by GC/MS. Kotianová et al. (2004) reviewed organics in aerosols analyses, which presented the procedures and methods used for identification of organic compounds in the particulate matter, showing that GC-MS is one of the most widely used techniques to separate, identify and quantify individual species within aerosol particles. Compared with the traditional solvent extraction method, direct thermal desorption analysis has the advantage of lower detection limits under most conditions. The thermal desorption method also avoids the complicated and time-consuming sample handling process and possible contamination from the solvents. The thermal desorption method has most often been used for non-polar organics as compared with polar organics (Welthagen et al., 2003). Goldstein et al. (2008) reported a new version of such an instrument used for the measurement of organic compounds in ambient aerosols, called 2D-TAG. It combines two dimensional GC (GC×GC) with the thermal desorption aerosol treatment. This instrument greatly improved the separation of organic compounds in the ambient

aerosols collected. In another study of TD-GC/MS, the authors used thermal desorption, cryofocusing, and GC/MS successfully to identify 60 target compounds from ambient particulate matters in Gold, BC, Canada (Ding et al., 2009).

Chemical analysis of ambient aerosols is important in identifying the sources, transportation and formation mechanism of these aerosols. Therefore, my scientific objective of this research is to characterize the chemical composition of aerosols, and try to relate the chemical to other aerosol properties. I will describe below the sampling conditions at the field sites studies, the sampling methods, and the instruments used for chemical analysis in the laboratory. The study's main focus is on the measurement of particulate matters emitted from animal feeding operations, and was designed to characterize selected chemical properties of both coarse and fine particles.

Raman Microspectroscopy (RM) is another analytical technique developed recently for the investigation of single particle composition (Takahama et al., 2007).It is a powerful technique to study chemical composition of atmospheric particles on a single particle basis. Recently, RM was used to create chemical maps of single atmospheric aerosols and pollen grains (Everall, 2000a and 200b; Sadezky et al., 2005; Lee and Chan, 2007; Tomba and Pastor, 2007; Schulte et al., 2008), this technique enables us to investigate the degree of internal mixing of multiple components in a single particle. RM and mapping have been applied for the analysis of soot, humic-like substances (HULIS) and inorganic compounds in size resolved samples of air particulate matter(Ivleva et al., 2007). Here, I applied RM for the investigation of atmospheric aerosol particles collected with PIXE Streaker sampler, explored the potential of this technique for qualitative analysis of soot, humic-like substances, organics and inorganic components in atmospheric particulate matter.

This study explored different chemical characterization methods of agricultural and urban airborne particulate matter. Three different field campaigns are discussed. For the agricultural aerosols, I report measurement of the chemical composition of size-resolved agricultural aerosols collected from a ground site at the nominally downwind and upwind edge of a feedlot in West Texas. High volume cascade impactor samplers

were used for the collection of the particles, and two major analytical methods were applied to characterize different components of the aerosols, ion chromatography (IC) was used to measure ionic composition with the main targets being ammonium (NH_4^+), nitrate (NO_3^-), and sulfate (SO_4^{2-}), direct thermal desorption gas chromatography-mass spectrometry/flame ionization detection (GC-MS/FID) methodology was used to identify and quantify organic compounds in the aerosol particles. For the urban aerosols, I report the measurement of mass, and the chemical composition of size-resolved aerosols collected from two different locations in Houston, analyzed by the thermal desorption GC-MS/FID method. The investigation of single particle composition using RM is reported as well: RM and chemical mapping techniques have been applied for the qualitative analysis of components in the samples of air particulate matter collected in downtown Houston.

CHAPTER II

METHODOLOGY

2.1 Sites Description and Sampling Setup

In June and July 2007, and July 2008, field studies were conducted in Tulia, TX, where 45,000 head of cattle are housed in an open air feedlot (2.6 km^2), called "Feedlot C", which is a representative open air feedlot run by the Texas Cattle Feeding Association (TCFA) operation (Hiranuma et al., 2008). An aerial of the feedlot is shown in Figure 1 (from Google Earth). Local weather conditions at Feedlot C are characterized by a semi-arid suptropical climate with diurnal variation in temperature and relative humidity, the latter peaking in the coolest hours of early morning (Mitchell et al, 1974). Cooler temperatures, lower relative humidities, and lower wind speeds usually occur in the afternoons and evenings, concurrent with increased cattle activity. Major dust events occur when dry, uncompacted manure accumulates on the feedlot surface and dust is suspended by hoof action of the active cattle (Razote et al., 2006).

In March and April 2009, another field study was conducted in Houston, Texas, which is the nation's 4th largest metropolitan area. I carried out one month of sampling from March 11 to April 11 in a typical urban neighborhood, on private property of the Greater Houston Transportation Company (*Yellow Cab*), which is in a mixed land use area of Houston, a few kilometers north of downtown, shown in Figure 2. It is surrounded by residential areas in three directions, two multi-lane commuter roads, a light industrial area, and a park. During spring sampling, PIXE Streakers were used to collect time resolved aerosol samples for offline analysis using RM.

In October and November 2009, a shorter field study was conducted at the same site. I carried out nine days of sampling in two typical urban neighborhoods, the *Yellow Cab* site described above, and at a second site located atop the Moody Tower (MT) student dormitory building on the University of Houston campus, approximately 5 km southeast of Downtown Houston and 10 km west from the western edge of the Houston Ship Channel (HSC) (Figure 2).

In the field, I sampled at two different locations next to feedlot C with size-resolving cascade impactors for later off-line analysis of particles in the laboratory. Figure 3 shows the particle samplers operated in the field with aluminum filters for the different size range, which were exchanged regularly and stored in a refrigerator for later analysis. A brief description of each off-line laboratory technique will be given in the next sections.

Two tripods extending to approximately 1.5 m above the ground were located at the nominal downwind and upwind site of the feedlot respectively. Each tripod was equipped with two impactor samplers, connected to a pump by two polyethylene tubes. Two samplers were run in parallel on each tripod, equipped with either Teflon or Aluminum filters respectively. Sampling was carried out simultaneously at the nominal upwind and downwind sides of the feedlot, and sampling intervals were either 24 or 48 hours according to the weather (and dust load) conditions; usually 24 hours for high aerosol load conditions and 48 hours for relatively clean conditions. The impactor samplers were operated at a flow rate of 9 L/min. In the field, flow was regulated with a mass flow meter to 9 L/min, because the sampler's impactor stages were calibrated to deliver the indicated cutoff-points at that flow rate. A homemade adjustable electronic feedback loop was employed using the mass flow meter output voltage in a negative feedback loop to drive power to two 12 VDC membrane pumps, one per sampler. Flow rate was checked and adjusted regularly during sampling.

A total of 150 size-resolved filter samples were collected during the sampling periods. At the end of each 24-h sampling period, all filter samples collected in the field were sealed in individual containers, shown in Figure 4, temporarily stored in a refrigerator, then transported in a refrigerated cooler to the Texas A&M College Station laboratory and again stored refrigerated until analysis. Several field blanks were also collected and analyzed in order to quantify the level of contamination during filter handling, shipping and analysis. The average concentrations of the field blanks were small, generally under the detection limit of the analytical systems, so I will not consider the contamination during sample collection further.

The same tripod setup equipped with two samplers as used during the West Texas field measurements was applied at both Houston locations, sampling at near-equal time intervals at both sites. The Moody Tower site is unique, as it can be affected by different air masses from urban, biogenic, and industrial sources throughout the Houston area.

2.2 The Sampling Systems

Our sampling setup consists of two white, weather-proof boxes that contain the DC-pumps with feedback controllers aspirating air through two ¼" OD polyethylene tubes, each tube connected with one cascade impactor sampler. As shown in Figure 5, we used a five-stage Personal Cascade Impactor Sampler from SKC Inc. (PCIS, Cat. No. 225-370) to sample particulate matters in the diameter ranges <0.25 μm, 0.25-0.5, 0.5-1.0, 1.0-2.5 and >2.5μm. Impact materials included 25 mm diameter Teflon and Aluminum filters, and a 37 mm diameter glass fiber as back-up filter. Each cascade impactor sampler consists of four impaction stages filled with the Teflon or Aluminum filters, followed by the glass fiber back-up filter.

Design and comprehensive laboratory evaluation of the PCIS were described in detail by Misra et al. (2002). Here I just give a brief description of the cascade impactor sampler that I used during two sampling campaigns. Each cascade impactor sampler consists of four impaction stages and an after-filter that allows the separation and collection of airborne particles in five size ranges (Figures. 5a–d). The sampling flow rate is 9 L/min, and the cascade impactor sampler is used in combination with a KNF sample pump (model PU 1215-N814-9.00). Particles in the size range of 0.25–10 μm are accelerated through rectangular-shaped nozzles and collected on Teflon or Aluminum filters with diameter 25 mm; particles smaller than 0.25 mm are collected on a 37 mm flow-through glass fiber back-up filter. Top-Trak® Mass Flow Meters (Sierra Instruments, Inc) were used to measure the mass flow rate of gases.

For mass and inorganic ion concentration measurements, the cascade impactor sampler substrates were Teflon filters. For organics analysis, aluminum foil filters were

used for the cascade impactor samplers. I compared relative mass sampling efficiency between different impaction materials during the West Texas field study, and variance between the same aluminum impaction materials/filters from the Houston field study, both as a function of particle size, by operating samplers in parallel. Results will be discussed below.

PIXE Streakers (http://www.pixeintl.com/Streaker.asp) were used to collect time resolved aerosol samples for offline analysis of RM. As shown in Figure 6 a, two Streaker Samplers were equipped on a protective instrument housing 2 m above the ground, which were used for continuous collection of particles at this location. The Streaker produces a continuous series of discrete samples for offline chemical composition analyses. With an air flow of one liter per minute, particles are collected in the size range of PM_{10} on 82-mm diameter aluminum filters. Figure 6 b shows a cross-sectional view of PIXE Streaker sampler configured for two size-fraction operation. Arrows indicate airflow. Sampling intervals were set to 25 minutes for continuous daily collection at the sampling site, and regular change of filter wheels occurred twice every week. The aluminum foil was used as the particle impaction and sample substrate, all samples collected in Houston were transported in a refrigerated cooler to Texas A&M University and stored under refrigeration until analysis by RM.

2.3 Mass Measurements and Subsequent Sample Pretreatment

For mass concentration measurements, all 25-mm impactor filters were weighed before and after each field sampling using a Sartorius Electric Micro-balance (model LE26P, Sartorius Inc., Germany) in the laboratory. The balance was placed in a reinforced plastic chamber (Figure 7), in which environmental conditions – specifically relative humidity – was controlled with a saturated salt solution (K_2CO_3, constant 45% relative humidity in air above this saturated solution). Temperature and humidity inside the balance chamber were monitored by a data logger (HOBO Data Logger, Onset Computer Corporation); by controlling the relative humidity in the chamber, we can

reduce the influence of humidity on aerosol particles. In addition, the setup was placed on a marble table to minimize vibrational influences.

Filters loaded with particulate matter were weighed, humidity equilibrated for minimum one hour, and reweighed again. After weighing, the Teflon and glass fiber filters were moved into 2 mL polyethylene vials, 1.5 mL high purity water was added and the vial was subjected to water extraction in an ultra-sonic bath (Cole-Parmer instrument Company standard sonicator). The water extracts were stored in a refrigerator until ion chromatography analysis, as described below.

The aluminum filters were analyzed without pretreatment by thermal desorption gas chromatography–mass spectrometry/flame ionization detection (GC-MS/FID). To test the Al filters for out-gassing or other chemical changes, I performed a heating test in the laboratory: I weighed the aluminum filters, then baked them at 200 °C inside an oven for about 2 hours, then reweighed them when they were cooled down. Results showed that there was no obvious difference of the filter mass, as shown in Figure 8.

To evaluate the precision and reproducibility of the balance, the same blank aluminum filter was measured in the same way described above for six times in six hours, and I calculated the standard deviation for comparison to the manufacturer's specifications of the balance's performance. Results showed the standard deviation is around 2.34 μg, close to the manufacturer's precision of ±2 μg for this balance.

2.4 Ion Analysis

Ionic components of the sampled aerosols were determined from 75 Teflon and glass fiber filters. As briefly discussed above, the Teflon and glass fiber filters were extracted with deionized water after weighing, immersed in Millipore water, and subjected to sonication for 15 minutes. The extracts were sealed in their individual vials and stored in a refrigerator until analysis. The extracts were analyzed for cations and anions using an older model Dionex Ion Chromatograph system (Dionex system 4000i). The main target of cation analysis was ammonium (NH_4^+), and the anionic targets were sulfate (SO_4^{2-}) and nitrate (NO_3^-). For the cation analysis, separation was achieved on a

25 cm long Dionex IonPac CS12 cation exchange column with 18 mM methane sulfonic acid (MSA) as eluent and a flow rate of 1.0 mL/min. 100 mM tetrabutylammonium hydroxide was used as the cation regeneration solution as specified by the supplier. An ammonium sulfate solution was used as standard stock solution for obtaining a standard calibration curve using dilutions. Identification of cations was based on retention time as compared to the standard. Figure 9 showed a sample chromatogram of cations analysis which give the detection limits of ammonium according to the related calibration curve. Based on the retention time compared to the standards, we can see some other ions such as Sodium, Potassium and Calcium ions were also detected but not quantified, further analysis is needed for the quantification of these cations. The peak area of ammonium (peak 2) in Figure 9 is 6936990 uS^2, around 5 times the detection limitation, so the ammonium concentration in this sample is about 1.26 ppm.

The anions were determined on a 25 cm long Dionex AS4A-SC column using 1.8 mM Na_2CO_3/1.7 mM $NaHCO_3$ as eluent solution and a flow rate of 0.5 mL/min. Sodium sulfate and sodium nitrate stock solutions were used to obtain standard calibration curves.

For all analyses, 1 μl of each standard solution was directly injected into the instrument. Solution blanks containing only 0.1 M HCl were also analyzed by ion chromatography to determine if there was any ammonia emanating from the tubing and filters, and none was detected.

Ion chromatography can be used to determine the water-soluble inorganic components in aerosol particles. One disadvantage of using ion chromatography is that this method consumes a significant amount of eluent and regeneration solution, and daily replacement of these solutions was necessary, and a new calibration was required each time the solutions were changed.

2.5 Thermal Desorption GC-MS/FID Method

A direct thermal desorption method followed by gas chromatographic separation and MS/FID detection was used to identify and quantify organic compounds in

atmospheric aerosols. All aluminum filter particle samples were analyzed by thermal desorption GC-MS/FID method. In the laboratory, small strips of each aluminum filter exposed to depositing particles were cut from the 25 mm filter and packed into a Siltek-deactivated (Restek Corp., proprietary), gooseneck inlet liner that fits into the standard HP 5890 gas chromatograph injector. Organics on the filter that can be thermally desorbed in the injection port and are of low volatility, were focused onto the head of a GC column for subsequent separation and detection. Compounds eluting from the column were split between a flame ionization detector (FID) and mass selective detector (MSD) to provide simultaneous mass spectral identification and FID quantification. Data were acquired and processed with HP Chemstation software. Individual compounds were identified by comparison of their mass spectra with mass spectral library data, and by comparison of mass spectra and GC retention times with known standards. Just as for the ion analysis, blank filter samples were also prepared and handled in the same way as field filter samples. Standard injections were used to determine the detection limits of the GC-MS/FID system.

Calibration curves were produced by the analysis of standard mixtures purchased from Restek Corporation, as shown in Table 1, both standard mixtures including 16 components. Calibration standards were prepared by spiking known amounts of the liquid standard mixtures (typically 0.5-2 μL) onto blank filter strips, which were placed into the inlet liners by tweezers and analyzed in the same way as for the sample filters. Liners were generally desorbed without a sample filter first to remove any adsorbed organics from the liner. Filter samples were dropped into the cold liner (typically 30-60 °C) through a “flip-top” fast to open and close injector head. Injection occurred through starting the chromatogram after heating the injector to its nominal setpoint of 300 °C. Heating rates and subsequent start of the oven temperature program were highly reproducible.

A stock solution calibration standard of PAH with a concentration 200 ug/mL was prepared in methylene chloride solvent. Five levels of calibration solution were prepared from the stock solution in order to make the calibration curves for all PAH

standards. I characterized the capability and reproducibility of the analytical setup with the standard mixtures. I checked the reproducibility of the method by injecting the same amount of standard mixture repeatedly, and I determined evaporative losses from the filters by comparing direct injection at cold or hot injector temperatures. Gloves were worn and all liner tubes and filters were handled only with clean forceps to avoid any contamination of the outer portion of the tubes. A blank tube was run before each analysis to avoid any potential contamination due to carry-over from the previous analysis. The liner in the injection system was packed with glass wool which may have prevented heavy and polar compounds from entering the GC column (Ding et al., 2009).

Chromatographic separation was achieved on a 60 m RTX-5ms column equipped with a 5-m pre-column to aid in sample focusing. Helium or hydrogen were used as carrier gas with optimal flow rate settings guided by the HP Chemstation software, usually a constant flow rate between one and two milliliters per minute. The temperature program was 30 °C for 1 min, increased at a rate of 12 °C/ min to 320 °C, and then held at the final temperature of 320 °C for 10.83min, for a total run time of 36 min. Samples were analyzed under the same chromatographic conditions as the standard solutions.

2.6 UV-is Method

After the ionic analysis completion, I attempted a UV-vis spectral analysis measurement with the aqueous samples in assessment of the light-absorption properties of any dissolved organics in my samples. I used a standard UV-vis spectrometer with acrylic, square cuvettes of 1 cm side length. First, I tested the absorption of a blank cuvette, then a cuvette with water, and then a cuvette with aqueous sample extract to check whether there are obvious absorption lines in the 200- 600 nm range. Results showed that there was a measurable difference between the latter two for the extract from high mass samples. The maximum absorptivity was observed near 294.5 nm. Subsequently, I made standard humic acid solutions of different concentrations and scanned at the wavelength 294.5 nm for calibration. Using the standard curve, I

attempted to determine the mass of water soluble organics in the samples. I did not obtain conclusive results for this measurement.

2.7 Raman Microspectroscopy Analysis

DXR Raman Microscope Apparatus (Thermo Fisher Scientific Inc.) was used for analysis, which was equipped with an Olympus BX microscope with a 50 × objective (LUMPlanFl), 25 μm confocal aperture, a motorized *x*, *y*-stage, and a charge-coupled device (CCD) detector. The 532 nm line of a Nd:YVO_4 Diode-pumped solid state (DPSS) laser was used as the excitation source, with maximum laser output power of 10 mW. Raman spectra of the aerosol samples were recorded over the spectroscopic range of 50 to 3500 cm^{-1}, with a spectral resolution of ~7.5 cm^{-1}.

Raman Microspectroscopy (RM) is an inelastic light scattering experiment that measures the vibrational frequencies of the sample and provides fingerprint spectra of molecular structures and compositions, and information about internal and external mixtures. Raman Microspectroscopy used in this study quantifies the inelastic scattering between the monochromatic laser beam light (532 nm in wavelength) and the molecular bond's ro-vibrational transitions within single particles (Skoog et al., 1997). The laser light interacts with phonons in the molecule, resulting in the energy of the laser photons being shifted up or down. The shift in energy gives information about the phonon modes in the molecule. Figure 10 illustrates the theory of Inelastic Scattering. When an incoming photon beam interacts with a molecule, it can get scattered without changing its energy, i.e. Rayleigh scattering, or it may exchange energy with distinct ro-vibrational states, either exciting ground states to lower ro-vibrational states (Anti-Stokes Raman scattering) or de-exciting populated higher energy states to higher ro-vibrational states (Stokes Raman scattering). The energy between the original state and the resulting new state is different for distinct molecular bonds and functional groups, therefore molecular compositions can be identified by Raman Microspectroscopy.

For the analyzed samples, the mapping was conducted over three different 50 μm × 50 μm areas on each deposition spot using a step of 5 μm and an exposure time of 10

s, so one hundred Raman spectra were obtained in each 50 μm × 50 μm area, and a total of three hundred spectra were collected on each deposition spot. The mapping procedure was employed in this study with reference to the technique reported in a previous study of atmospheric aerosols using RM (Ivleva et al., 2007). Spectral maps are created by a computer-controlled mapping procedure, in which the precision motorized *x, y*-stage is moved with respect to the microscope objective in incremental steps (5 μm) in the *x* and *y* directions respectively. Most spectra in the map represent a single independent particle, however, a few agglomerations that were large enough were observed occasionally in multiple spectra. Table 4 summarized Raman frequencies observed in spectra of agricultural aerosols and their tentative assignments to the classes of vibrational modes (from PhD thesis by N. Hiranuma, TAMU, 2010).

Raman spectra of some salts, organics and HULIS – as typically found in aerosols – are shown in Figures 24 a-c. These spectra were created by analyzing the standard reagents, for example, the salts of NH_4NO_3, $(NH_4)_2SO_4$, Na_2CO_3 $NaHCO_3$, $NaNO_3$ and Na_2SO_4 were used without further purification. All of the salts were dispersed on the foil filter for investigation, and the mapping experiment was conducted with a laser power of 4mW. The same procedure was employed for organics and HULIS standards.

CHAPTER III
RESULTS AND DISCUSSION

3.1 Total Particle Mass Concentration of West Texas Samples

Relative mass sampling efficiency between two different impaction materials for the West Texas field study was compared. The total particle mass concentrations obtained by impactor samplers with aluminum filters and Teflon filters were plotted in Figure 11 a. Regression was performed with either filter data on the *x*-axis because both measurements contain errors and a bivariate regression is needed. As each sample's error is based on the same mass measurement method, a geometric mean between the calculated OLS (ordinary least squares) slopes describes the relationship satisfactorily and without bias (Robert R. Sokal, 1981). The geometric mean regression slope in this case was 0.79, smaller than one, suggesting that the Teflon filters were more efficient in particle deposition, consistent with the developers' work (Misra et al., 2002). Figure 11 b shows a stage-by-stage statistical comparison of mass collection efficiencies for Aluminum and Teflon filter respectively, the geometric mean regression slopes are 0.87, 0.70, 0.91 and 0.45 respectively for stage one to stage four of two impactor samplers equipped at the nominal downwind site of the feedlot. Correlation coefficients are only 0.2848 and 0.4878 for stage three and stage four, that is larger uncertainties for ultra-fine particulate matter were found for both Teflon and Aluminum filters.

3.2 Ammonium, Sulfate and Nitrate Measurements

Figure 12 presents the average mass concentration of NH_4^+ compared to the total particle mass concentration at each stage of the sampler measured during the field experiment as a function of particle size in terms of collection stage number. We can see that most of the particle mass was in the coarse mode (>2.5 μm), and NH_4^+ mass concentrations were significant in the size ranges >2.5 μm and 0.25-0.5 μm. This means that some ammonium was found in the coarse mode particles and some in accumulation mode particles. The latter is an expected finding based on gas to particle conversion being the dominant process converting ammonia into particle ammonium. Particle

ammonium is formed from the reaction of gas-phase ammonia (NH_3) and some acid, the conversion of gas-phase ammonia to the particulate phase depends on air temperature, humidity, precipitation, and the presence and composition of preexisting particles. Hiranuma et al. (2008) stated that the relative humidities during the measurement campaign (usually <75%) limit the conversion of ammonia to the condensed phase ammonium. More measurements are needed to quantitatively understand the variability in observed ammonium concentrations.

As shown in Figure 12, in each size range, ammonium constituted only a minor fraction of total mass. This result agreed well with the research of Hiranuma (2010), which illustrated that the ambient NH_3 at the feedyard is almost completely found in the gas phase. I compared my results of ammonium concentration from particulate matters collected in 2007 at the same field sites to the studies of Hiranuma (2010), which showed an average of 1114 ppbv and 33 ppbv NH_x (i.e. total gas phase plus particle ammonium) at the downwind and upwind sites respectively, and average gas-phase NH_3 mixing ratios of 1063 ppbv (downwind) and 31 ppbv (upwind). Converting average ammonium concentrations in particulate matter from ion analysis shown in Figure 12, lead to 0.74±0.44 (average ± 1 sd) and 0.35 ± 0.2 ppbv downwind and upwind sites respectively. This may be low by as much as a factor of 2 as the back-up filter was not analyzed. Results are compared in Figure 13 using 2007 average differences between NH_x and gas-phase NH_3 (Hiranuma, 2010). The comparatively low values of aerosol ammonium when converted to gas-phase ammonia confirm that Hiranuma's (2010) measurements could not have revealed any significant differences between total and gas-phase ammonium, so that these results create a consistent picture. Note that in some samples, the concentration of particle phase ammonium was even below the detection limit of the ion analysis, indicating that within the uncertainty of ion measurement (±10%), no detectable ammonium was in the particle phase.

Figure 14 shows the average ammonium (NH_4^+), sulfate (SO_4^{2-}) and nitrate (NO_3-) mass concentrations measured on the four-stage impactor and back-up filters, based on a total of 50 Teflon and glass fiber back-up filter samples obtained from the

downwind site of the feedlot. (no ammonium mass concentrations were measured on the back-up filter). Results showed that SO_4^{2-} was the main ionic component in the aerosol particles, especially in the size range <0.25μm, as expected.

To compare the possible impacts of ammonia emissions from the feedlot on particle composition, I compared the concentration of aerosol NH_4^+ between the nominal downwind and upwind locations. Figure 15 a demonstrates that, although low, NH_4^+ concentrations at the downwind site were significantly higher compared to upwind NH_4^+. Interestingly, the same was found for sulfate (as shown in Figure 15 b) and nitrate. Figure 15 a also shows that most NH_4^+ mass was found in the size ranges > 2.5 μm, and 0.25 - 0.5 μm, NH_4^+ in accumulation mode particles is an expected finding. The difference in the size range 0.25 - 0.5 μm may be attributed to the gas to particle conversion, which is the dominant process converting ammonia into particle ammonium.

3.3 Total Particle Mass Concentration of Houston Samples

Variations between the same impaction materials were studied for the Houston field samples by running two impactor samplers with the same aluminum filters in parallel at the Yellow Cab and Moody Tower sites, respectively. The total particle mass concentrations were plotted in Figures 17 a-e and Figures 18 a-e along with linear regression lines. These Figures show that mass concentrations on the filters of the first two stages were highly correlated with correlation coefficients of $R^2 = 0.94$ and $R^2 = 0.96$, while weaker correlations were found on the third and fourth stages, at both sample sites. The results were shown tabulated in Table 2, which summarize the geometric mean regression slopes and the regression coefficients for Yellow Cab and Moody Tower, respectively. The results show that a good reproducibility (better than 10-20%) can be achieved for coarse and accumulation mode particles, while fine particle mass determination is less accurate, at least in part due to limitations set by the balance (±2 μg resolution only).

I also compared the effect of sampling time length between samplers: I operated one sampler at the Yellow Cab site sample for 29 h (from 1PM on Nov 2 to 6PM on Nov

3) and another sampler for 19 h (from 1PM on Nov 2 to 8AM on Nov 3) and 10 h (from 8AM to 6PM on Nov 3) separately. Figure 16 a shows that the total particle mass of the 29-h sample was almost equal to the total mass particle mass of 19 h plus 10 h samples, for total mass and between the different stages. The same test was done at the Moody tower site, this time running one sampler for 46 h and another one for 22 h and 24 h. Figure 16 b shows the respective comparison with a similar result as at the Yellow Cab site.

3.4 Organics Analysis

Calibration Curves were constructed by plotting the most abundant mass or the peak area (from TIC) between the analytes versus the injected amount of the analytes. In the laboratory I injected the PAH mix calibration standard with a concentration of 200 µg/ml three times at each volume of 0.5 µl, 1.0 µl, 1.5 µl, 2 µl. Figure 19 presents examples of the resulting calibration curves of three PAH standard mixtures indicated by dominant mass abundance (left) and TIC peak areas (right) versus mass of PAH standard solution injected on the filters. Figure 19 c shows an example of a poor PAH calibration.

Figure 20 shows sample total ion chromatograms (TIC) with identification from a West Texas feedlot sample. Figure 20 a shows the analysis of the filter on stage one and Figure 20 b shows the analysis of the combined filters on stages 2-4. Generally, only small mass amounts were collected on the fine aerosol stages, and filters were combined for analysis to increase sensitivity. Aerosol mass was usually sufficient for the coarse mode particles. Figures 21 a-b show total ion chromatograms of soil samples (dominantly dried manure) from the West Texas feedlot. Some acids such as Hexadecanoic acid and Octadecanoic acid were both identified in the fine and coarse soil samples. There also is a general similarity between the TICs in Figures 20 and 21.

Table 3 listed some results of VOCs analysis for the samples collected on the Aluminum filters from West Texas, some dominant organics such as C16 acid and C18 acid were investigated, and the percentage of total observable organics were also studies by integrate the sum of all FID area counts. Results show the abundance of the dominant

organics such as C16 acid and C18 acid constituted ~0.5 % and ~1.4 % by mass of the total particle mass on the filters respectively. The relative mass of all detectable compounds was investigated by integrating all FID area counts; the total observable organics account for ~5.6 % of total particle mass on the collected Aluminum filters.

For the Houston urban samples, long-chain alkanes and PAHs were targeted and quantified, also in this case, filters were split between coarse (> PM 2.5) and fine mode (PM 2.5) particles. However, the detection limits of our system were often not low enough to quantify organics abundances in my samples.

3.5 Raman Microspectroscopy Analysis

Chemical composition of the particles has been observed on single particle basis using Raman Microspectroscopy (RM). Since RM is a high resolution but time consuming technique, only three sets of samples that have been collected in the midnight, morning rush hour and noon Mar 21, 2009 were investigated in detail. On the substrates obtained in the morning Mar 21, three deposition spots (50 μm × 50 μm per spot) have been mapped at laser intensity 1mW, 4mW and 8mW respectively to study the spatial variation in composition with different laser intensities, so a total of nine hundred spectra were created for the morning samples of Mar 21. For the midnight sample of Mar 20 and noon sample of March 21, three deposition spots were mapped at an excitation laser power of 8 mW respectively, so a total of six deposition spots were mapped.

As can be seen in Figure 23 A, a Raman spectrum was collected at each of the point grid on the microscope map. Multiple particles were collected and imaged in this sample. Next spectra were sorted and major peaks were identified. For example, the Raman spectra of several particles (I, II, III, IV, V and VI) with the major peaks were identified and shown in Figure 23 B. Each of these particles in this sample has different major components. Particles II, IV,V and VI were mainly composed of Calcium Carbonate ($CaCO_3$), Sodium Nitrate ($NaNO_3$), Ammonium Nitrate (NH_4NO_3) and Calcium Sulfate ($CaSO_4$) respectively, the major components of particle I were soil/soot

dominant complex with sodium nitrate ($NaNO_3$) at ~1068 cm^{-1}. The broad peak at ~1500 cm^{-1} indicates the presence of amorphous carbon (Sadezky et al., 2005), which is the main component of Particle III.

Raman spectra can also be used to investigate the degree of internal mixing of multiple components in a single particle. The observation of single and multi-component spectra indicated the presence of both externally and internally mixed particles. For example, the spatial distribution of each component in all particles is mapped in Figure 24, in which the integrated area of a single chosen spectral peak is mapped. Maps of the integrated area of individual peaks, $CaCO_3$, amorphous carbon, $NaNO_3$, NH_4NO_3 and $CaSO_4$ are shown in Figure 23 A, B, C, D and E respectively. This gives an indication of the degree of internal and external mixing. For instance, particle I showing up in all the five spectral maps indicates that particle I is the combination of five components. Particle II shows up in spectral map C, which indicates that the particle contained $NaNO_3$. In contrast, Particle III shows up in spectral map B but not the other maps, which indicates that particle III is predominantly composed of amorphous carbon. Figure 25 shows representative Raman spectra of internally mixed particles. For example, Figure 25 A shows a representative Raman spectrum of an inorganic dominant complex with $CaSO_4$ at ~1006 cm^{-1} and $Ca(NO_3)_2$ ~1050 cm^{-1}, Figure 25 B shows a representative spectrum of a soil/soot dominant complex with HULIS bands at ~1500, Na_2SO_4 at 995 cm^{-1} and NH_4NO_3 at 1045 cm^{-1}.

A total of 1500 spectra were recorded for analyzed particles collected at Yellow Cab location. The results are summarized in Table 4 and Table 5 respectively, the total number of spectra recorded per invested filter range from 48 to 176 depending on laser intensity and sampling time. All peaks > 50 counts per second (cps) were considered to be major components. A detailed method was developed to categorize single particle data by Raman MS. As seen in Figure 22, after all the measurements were done, spectra were qualitatively classified into several groups manually based on our understanding of chemical similarity. Four categories were used to classify all the 1500 spectra based on similar spectra features. First category of spectra type, namely “Organics”, include the

complex combination of characteristic Raman bands contributed from saturated fatty acid and specific organic chemical bonds corresponds to applied energy. The "inorganics" types classified in Table 4 and Table 5 include sodium sulfate (Na_2SO_4), calcium sulfate ($CaSO_4$), ammonium nitrate (NH_4NO_3), calcium nitrate ($Ca(NO_3)_2$), sodium nitrate ($NaNO_3$), sodium carbonate (Na_2CO_3) and calcium carbonate ($CaCO_3$), the fraction of these kind of particles appeared to decrease with the increase of laser intensity. Third, any combination of inorganic peaks and organics was grouped as "inorganic dominant complex" type. Representative Raman spectrum of this group is shown in Figure 24A. Lastly, the most dominant type of spectra was categorized into "soil/soot dominant complex", particles in this category were characterized with the presence of amorphous carbon that coincides with broad spectra from 1050 to 1620 cm^{-1}. These types of particles generally consist of multi-components and are internally mixed with the threshold of Raman intensity 50 counts per second (cps), as shown in Figure 24 B. Except the four major categories described above, the peaks at Raman shift around 100 cm^{-1} were observed occasionally, these peaks are the contributions of lattice vibration in crystals (Bougeard et al., 1977). The qualitative classification of spectra types is described below.

Table 5 summarized detailed chemical components of aerosols obtained in morning March 21, 2009, three deposition spots have been mapped respectively for three different laser intensity of 1 mW, 4 mW, 8 mW. A total of 900 spectra collected in the morning sample were analyzed, the total number of characteristic spectra for the particle deposition spots increased from ~48 to ~176 with the increase of intensity from 1mW to 8mW. The relative standard errors between the different spots investigated on this filter were no more than 4%, indicating fairly uniform composition and reasonable counting statistics. The ratio of the total number of recorded spectra over the total number of spectral scan per subset varied from ~16% for the particle deposition spots with 1mW to ~58.7% with 8mW. On the filter obtained at midnight of Mar 20 and noon of Mar 21, three deposition spots have been mapped at the laser intensity 8mW respectively, A total of 600 spectra collected at midnight and noon were analyzed, and the ratios of the total

number of characteristic spectra over recorded spectra for the three different time midnight, morning and noon samples are 44%, 58.6 % and 33% respectively. The results were summarized in Table 6.

As can be seen in Table 5, the percentage of organics from the sample collected in Mar 21 morning increased from 1.3% to 13.5% with the increase of laser intensity from 1mW to 8mW, while the percentage of inorganics decreased from 16.8% to 3.8%. The increase in organics fraction may imply that organics identified are Raman active at a higher range of laser intensity and the increase in detected organics population may have influenced the relative fraction of other compounds as well as measurement uncertainties among different intensities. Among all the mean spectral data subsets in the morning Mar 21, the contributions of soot/soil dominant complex were especially high: more than 70%, specifically, counting 76.6 ± 3.6%, 72.5 ± 0.7% and 74.8 ± 0.2% of the total spectra at 1mW, 4mW and 8mW respectively. Among all the inorganics, counting 16.8 ± 1.9% at 1 mW, $CaSO_4$ at 1006 cm^{-1} and $Ca(NO_3)_2$ at 1051 cm^{-1} were the most dominant components. $Ca(NO_3)_2$ is an important component of atmospheric aerosols; it has been confirmed that $CaCO_3$ particles in the atmosphere can be converted to $Ca(NO_3)_2$ (Sullivan et al., 2007; Liu et al., 2008).

From Table 5 and Table 6, we can see that the fraction of soot/ soil dominant complex was the most prevalent composition in analyzed samples. For the soot/soil dominant complex categories, soot/soil represents a large percentage of the total particles, decreasing from 72.9% to 48.9% with the increase of laser intensity in the analyzed sample of Mar 21 morning. This agrees with the decrease of the inorganic percentage, as it leads to an increase of the inorganic components in the soot/soil dominant complex. As can be seen in Table 5, a highly complex mixture of inorganic compounds can be found as a part of soil/soot dominant complex particles. Table 6 compares the samples collected in the midnight, morning and noon time at 8mW: We observe that the “soil/soot dominant complex” was still the most dominant type of spectrum, quantitatively counting for 70.0 ± 0.8%, 74.78 ± 0.2% and 30.9 ± 1.6% of total spectra for midnight, morning and noon samples. Soot/HULIS was the most

dominant component of the "soil/soot dominant complex" samples. More soot/soil components were found in the sample obtained in the morning, counting for 48.9 ±1.1% of total spectra, and there were more multi-component in the sample obtained in the midnight, counting ~30.4%. Sodium nitrate was not observed in the sample obtained in the morning, while the percentage of sodium nitrate was 21.9 ± 1.7% of total spectra in the noontime sample.

Raman spectra of various components were influenced by laser power. For comparison, spectra at different intensity (1 mW, 4 mW and 8 mW) were collected to investigate any variations of Raman band with the laser excitation. For example, certain organics such as the amorphous and graphitic carbon peaks fluoresce significantly with laser power and it was also found that some of atmospherically relevant organic substances, such as polycyclic aromatic hydrocarbons (e.g., Anthracene and Pyrene) and humic-like substances (e.g., Pahokee Peat Soil II) were only detectable below 80 mJ (i.e., 8 mW x 10 s) of laser intensity. Figure 27 shows the Raman spectra of Glutaric acid as function of laser intensity at 1 mW, 4 mW and 8 mW. The increase of organics fraction in Table 5 may imply that organics identified are Raman active at higher range of laser intensity. Figure 26 shows characteristic Raman spectra of the reference materials for HULIS (Graphite, Fluka standard Humic Acid, Pahokee Peat Soil II, and Leonardite). They all show peaks at ~1350 cm^{-1} and ~1580 cm^{-1}, but these two peaks differ greatly with respect to relative intensities and widths.

CHAPTER IV
SUMMARY AND CONCLUSIONS

This study focused on the chemical characterization methods of agricultural and urban airborne particulate matter (PM) collected during two different field campaigns. For the agricultural aerosols, the measurement of mass and the chemical composition of size-resolved PM collected at the nominally downwind and upwind edge of a feedlot in West Texas were reported. Off-line analysis of field samples was performed using a standard ion chromatography method to determine the ionic components of particulate matter. It was found that most of the particle mass was in the coarse mode (>2.5 μm), and NH_4^+ mass concentrations were significant in the size ranges >2.5μm and 0.25-0.5 μm. The latter is expected as particle ammonium is usually formed from the reaction of gas-phase ammonia (NH_3) and some acid, called gas-to-particle conversion. This conversion of gas-phase ammonia to the particulate phase in the air depends on air temperature, humidity, precipitation, and the presence and composition of preexisting particles. The relative humidities during the measurement campaign (usually <75%) limit the conversion of ammonia to condensed phase ammonium. Comparisons of the average mass concentration of ammonium to the total particle mass concentration at each stage of the sampler measured during the field experiment were made. Results showed that the concentration of aerosol ammonium was low, and it constituted only a minor fraction of total mass. Previous gas-phase and total ammonium at the site showed that the ambient NH_3 at the feedyard is more or less exclusively in gas phase, but elevated at the downwind compared to the upwind location. In this study, low particle ammonium confirmed this finding but also showed that particle ammonium nevertheless about doubles between the up- and downwind locations.

Total particle mass concentrations measured by impactor samplers with Al filters and Teflon filters were compared, showing good correlation but lower collection efficiency on the Al filters. Anion analysis showed aerosols were acidic; nitrate and sulfate represented the major part of the aerosol ionic composition. For the urban aerosols, I compared measurements of mass between the Al filters and showed that

reproducibility is high except for the fine PM, for which low mass amounts were collected that are difficult to measure accurately on the available microbalance.

Organics analysis did identify several hydrocarbons and VFAs in the samples, with C16 and C18 acids dominant. Sterols were also identified in some samples. However, detection limits were generally not low enough to quantify organics abundances in 24-h samples, many samples showed no or very few peaks, and large aerosol masses were needed for identification of more volatile and semi-volatile organics.

For the samples collected over the sampling period with Aluminum filter in West Texas, organics analyses shown the abundance of the dominant organics such as C16 acid and C18 acid constituted ~0.5 % and ~1.4 % by mass of the total particle mass on the filters respectively. The relative mass of uncertainty compounds was investigated by integrating all FID area counts, the total observable organics account for ~5.6 % of total particle mass on the collected Aluminum filters.

Measurements of single particle compositions were performed using RM, the results of Raman mapping experiments with different laser intensity provide quantitative information about the composition and mixing state of aerosol samples. The major component of aerosols at the Houston urban sampling location was soot or “soil” material (HULIS) in ~70% of the particles analyzed in the morning and to a lesser extend in the samples at noon: ~ 30.88% of total spectra of samples. Particles containing other organics comprised an additional ~10% of the total particle population with high population of 23.2% at noon. High fraction of inorganic (23.2% of total population of the sample) was found in the sample collected at the noon Mar 21.

In conclusion, this study focused on the chemical characterization methods of agricultural and urban airborne particulate matter. Three main different measurement methodologies were employed, and each technique has its own advantages and disadvantages. Ion chromatography can be used to determine the water-soluble inorganic components in aerosol particles. The major limitation of ion chromatography is that it will introduce additional measurement uncertainties. This method consumes a significant

amount of eluent and regeneration solution; daily replacement of these solutions was necessary, and a new calibration was required each time the solutions were changed.

Organic compounds analysis with thermal desorption GC-MS can be used to identify and quantify individual organic compounds in particulate matter (PM) samples, which is an alternative to solvent extraction for many organic compounds, and is a relatively fast, simple, and sensitive analytical method compared to solvent extraction. For this method, thermal stability of organic compounds is also important. Organic compounds in aerosol samples are separated according to their physical and chemical properties. Not all types of substrates are suitable for high temperature desorption, and the desorption temperature is directly related to the volatility and thermal stability of the targeted analytes. At desorption temperatures < 275°C, some analytes are not completely extracted, especially less volatile compounds. Temperatures higher than 340°C may cause thermally labile compounds to decompose. For both ion chromatography and thermal desorption GC-MS methods, the amount of aerosol mass sampled and the resulting detection limits are important, and low detection and quantification limits are needed for daily or better time resolution measurements. Only dominant, single chemical components in the aerosol can be analyzed this way unless a very high sensitivity MS is available.

Compared to Desorption GC-MS method, Raman Microspectroscopy can be used to obtain more detailed chemical information on a particle by particle basis. Raman mapping experiments can provide qualitative information about the composition and mixing state of aerosol samples. With RM we can find molecular specific information and get more detailed composition analysis, however Raman analysis is time consuming, which limits the number of samples that can be analyzed. To accurately quantify the abundances of organics components in the particulate matters, for thermal desorption GC-MS method, either high mass amounts are collected or low detection limits of GC-MS are needed. The observation of single and multi-component spectra indicated the presence of both externally and internally mixed particles. Further comprehensive and

systematic studies are needed for accurate quantitative analysis of atmospheric aerosols by RM and Raman mapping experiments.

To further explore the relationship between chemical composition and other physical properties, some modifications or improvements need to be made to the thermal desorption GC-MS and RM methods in the future studies of airborne particles. For thermal desorption GC method, instead of split of effluent between a MSD and a FID for compound identification and quantification, internal standards may be used as an alternative way of quantification on the MSD. Direct thermal desorption GC method should be used with respect to the large amount of samples acquired and the relative time consumption of GC-MS analysis. At the same time, all samples should be analyzed shortly after transferring back to laboratory to avoid sample storage time. With Raman we can find molecular specific information and get more detailed composition analysis, but the population of each composition varied in term of the laser density, to some extent, so a complementary analysis or combination is necessary.

REFERENCES

Bardouki H., H. Liakakou, C. Economou, J. Smolic, V. Zdimal, K. Eleftheriadis, N. Mihalopoulos (2003), Chemical composition of size resolved atmospheric aerosols in the Eastern Mediterranean during summer and winter, *Atmos Environ.,* 37, 195–208.

Brooks, S. D., M. E. Wise, M. Cushing, and M. A. Tolbert (2002), Deliquescence behavior of organic/ammonium sulfate aerosol, *Geophyiscal Research Letters*, 29, 1917.

Brooks, S. D., P. J. DeMott, and S. M. Kreidenweis (2004), Water uptake by particles containing humic materials and mixtures of humic materials with ammonium sulfate, *Atmos Environ.,* 38, 1859-1868.

Chan, M. N. and C. K. Chan (2003), Hygroscopic properties of two model humic-like substances and their mixtures with inorganics of atmospheric importance. *Environmental Science and Technology*, 37 (22), 5109-5115, 2003.

Ding, L.C., F. Ke, DKW Wang, T Dann, CC Austin (2009), A new direct thermal desorption-GC/MS method: Organic speciation of ambient particulate matter collected in Golden, BC, *Atmos Environ.,* 43, 4894-4902.

Faulkner, W.B. and B.W. Shaw (2008), Review of ammonia emission factors for United States animal agriculture, *Atmos Environ.,* 42, 6567-6574.

Goldstein, A. H., D. R. Worton, B. J. Williams, S. V. Hering, N. M. Kreisberg, O. Pani, and T. G´orecki (2008), Thermal desorption comprehensive two-dimensional gas chromatography for in-situ measurements of organic aerosols, *J. Chrom. A.,* 1186, 340-347.

Gysel, M., E. Weingartner, S. Nyeki, D. Paulsen, U. Baltensperger, I. Galambos, and G. Kiss (2004), Hygroscopic properties of water-soluble matter and humic-like organics in atmospheric fine aerosol. *Atmospheric Chemistry and Physics*, 4, 35-50.

Hiranuma, N., S.D. Brooks, B.W. Auvermann, and R. Littleton (2008), Using environmental scanning electron microscopy to determine the hygroscopic properties of agricultural aerosols, *Atmospheric Environment,* 42(9), 1983-1994.

Hiranuma, N., S.D. Brooks, D.C.O. Thornton, and B.W. Auvermann (2010), Atmospheric ammonia mixing ratios at an open-air cattle feeding facility, *J. Air & Waste Manage Assoc*., 60, 210-218, 2010.

Ho, S.S.H., J.Z. Yu (2004), In-Injection Port Thermal Desorption and Subsequent Gas Chromatography-Mass Spectrometric Analysis of Polycyclic Aromatic Hydrocarbons and *n*-Alkanes in Atmospheric Aerosol Samples, *J. Chromatogr. A.*, 1059, 121-129.

Ivleva, N.P., U. McKeon, R. Niessner, and U. Pöschl (2007), Raman microspectroscopic analysis of size-resolved atmospheric aerosol particle samples collected with an ELPI: Soot, humic-like substances, and inorganic compounds, *Aerosol Science and Technology*, 41, 655-671.

Kotianova, P., E. Matisova, H. Puxbaum, and J. Lehotay (2004), Analysis of organic compounds in aerosols, *A review, Chem. Anal.-Warsaw*., 49, 833–844.

Koziel,J.A., B.H. Baek, J.P. Spinhirne, and D.B. Parker (2004), Ambient ammonia and hydrogen sulfide concentrations at a beef cattle feedlot in Texas, In *Proc. ASAE/ESAE Annual International Meeting*. Ottawa, Ontario, Canada: ASAE.

Lee, A.K.Y. and Chan, C.K. Chan (2007), Single particle Raman spectroscopy for investigating atmospheric heterogeneous reactions of organic aerosols, *Atmospheric Environment,* 41, 4611-4621.

Merchant, J., A. Naleway (2005), Asthma and farm exposures in a cohort of rural Iowa children, *Environmental Health Perspectives*, 113(3), 350-356.

Miller, D. (2001), Accumulation and consumption of odorous compounds in feedlot soils under aerobic, fermentative, and anaerobic respiratory conditions, *Journal of Animal Science*, 79(10), 2503-2512.

Misra .C., M. Misra, S. Singh, P.M. Hall and C. Sioutas (2002), Development and evaluation of a personal cascade impactor sampler (PCIS), *Journal of Aerosol Science.,* 33, 1027–1047.

Mitchell, D. W., L. L. Jacquot, and R. B. Chance (1974), *Soil Survey of Swisher County, Texas.* United States Department of Agriculture, *Soil Conservation Service in Cooperation with Texas Agricultural Experiment Station*, Washington DC.

Ngwabie, N.M., G.W. Schade, T.G. Custer, S. Linke, and T. Hinz (2008), Abundances and flux estimates of VOCs from a dairy cowshed in Germany, *Journal of Environmental Quality*, 37, 565-573.

Parker, D.B., M.B. Rhoades, G.L. Schuster, J.A. Koziel, and Z.L. Perschbacher-Buser (2005a), Odor characterization at open-lot beef cattle feedyards using triangular forced-choice olfactometry, *Transactions of the ASAE*, 48(4), 1527-1535.

Parker, D.B., S. Pandrangi, L.W. Greene, L.K. Almas, N.A. Cole, A.B. Rhoades and J.A. Koziel (2005b), Rate and frequency of urease inhibitor application for minimizing ammonia emissions from beef cattle feedyards, *Transactions of the ASAE*, 48(2), 787-793.

Razote, E.B., R.G. Maghirang, B.Z. Predicala, J.P. Murphy, B.W. Auvermann, J.P. Harner, and W.L. Hargrove (2006), Laboratory evaluation of the dust-emission potential of cattle feedlot surfaces, *Transactions of the ASAE*, 49 (4), 1117-1124.

Rule, A.M., A.R. Chapin, S.A. McCarthy, K.E. Gibson, K.J. Schwab and T.J. Buckley (2005), Assessment of an aerosol treatment to improve air quality in a swine concentrated animal feeding operation (CAFO), *Environmental Science and Technology*, 39 (24), 9649-9655.

Sadezky, A., H. Muckenhuber, H. Grothe, R. Niessner and U. Pöschl (2005), Raman microspectroscopy of soot and related carbonaceous materials: Spectral analysis and structural information. *Carbon*, 43, 1731-1742.

Schicker, B., M. Kuhn, R. Fehr, L.M Asmis, C. Karagiannidis and W.H. Reinhart (2009), Particulate matter inhalation during hay storing activity induces systemic inflammation and platelet aggregation, *European Journal of Applied Physiology*, 105, 771-778.

Schulte, F., J. Lingott, U. Panne and J. Kneipp (2008), Chemical Characterization and Classification of Pollen, *Analytical Chemistry*, 80, 9551-9556.

Sin, D.W., W.H. Fung, C.H. Lam (2002), Measurement of carbonaceous aerosols: validation and comparison of a solvent extraction-gas chromatographic method and a thermal optical transmittance method, *Analyst,* 127, 614–622.

Singh, M., C. Misra, C. Sioutas (2003), Field evaluation of a personal cascade impactor sampler (PCIS), *Atmos. Environ.*, 37 (34), 4781-4793.

Skoog, D.A., F.J. Holler, and T.A. Nieman (1997), *Principles of instrumental analysis. 5th Edition.* Thomson Learning , London, UK.

Takahama, S., S. Gilardoni, L. M. Russell and A. L. D. Kilcoyne (2007), Classification of multiple types of organic carbon composition in atmospheric particles by scanning transmission Xray microscopy analysis, *Atmospheric Environment,* 41, 9435-9451.

Todd, R.W., N.A. Cole, N. Clark, T.K. Flesch, L.A. Harper and B.H. Baek (2008), Ammonia emissions from a beef cattle feedyard on the southern High Plains, *Atmospheric Environment*, 42(28), 6797-6805.

Welthagen W., J. Schnelle-Kreis, R. Zimmermann (2003), Search criteria and rules for comprehensive two-dimensional gas chromatography–time of-flight mass spectrometry analysis of airborne particulate matter, *J. Chromatogr. A.*, 1019, 233-249.

APPENDIX A

Figure 1: Map of Feedlot C in West Texas. Highlight the nominal upwind site (N 34°38.5' W 101°47.32') and downwind site (N 34º 39.5' W101º 47.3').

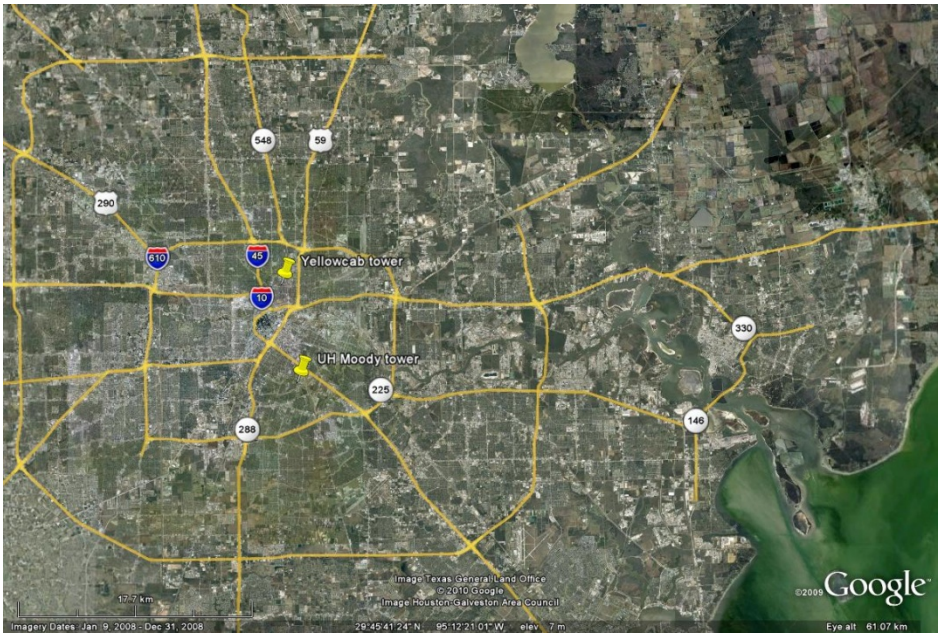

Figure 2: Locations of the investigated sites in the Houston metro area. Yellow Cab and Moody Tower.

Figure 3: Pictures of the Cascade Impactor Sampler with collected particulate on aluminum filters.

(a) (b)

Figure 4: Pictures of containers used for filter storage.

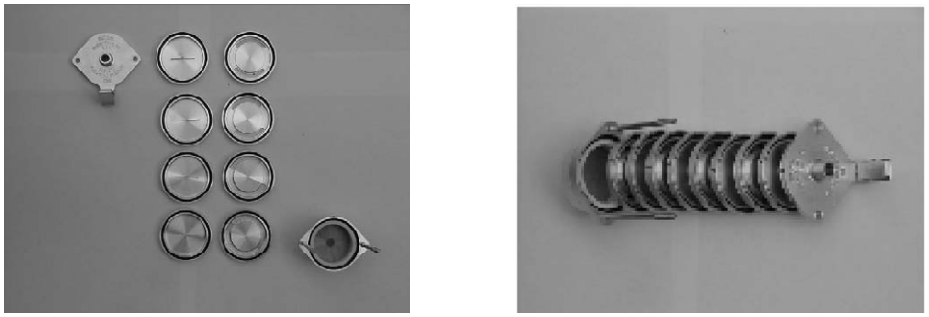

(a) (b)

Figure 5: Pictures of Personal exposure Cascade Impactor Sampler. (a) four impaction stages and one back-up filter, (b) disassembled sampler including inlet and outlet plate, (c) one of the impaction stages including accelerator plate(right) and collector plate(left), (d) overall picture of one PCIS with length only 3.4 inch(Singh, M et al., 2003).

(c)

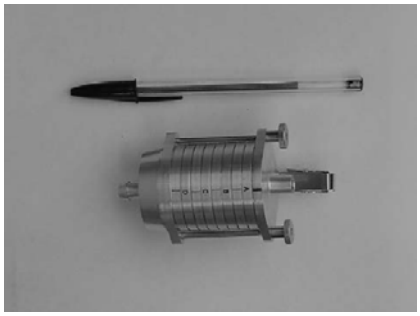

(d)

Figure 5 continued

(a)

PIXE Streaker

(b)

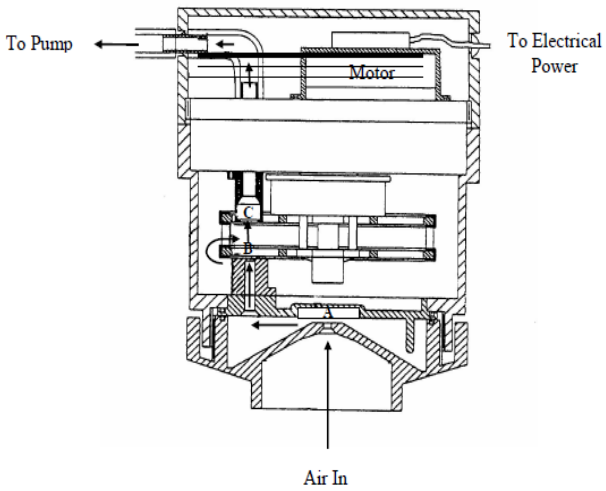

Figure 6: (a) Pictures of PIXE Streakers setup in field site and (b) Cross-sectional view of PIXE Streaker sampler configured for two size-fraction operation. Arrows indicate airflow. Air passes through the non-rotating pre-impaction stage A, where particles larger than 10 mm are deposited. The air then flows through an impactor slit B where particles larger than 2.5 mm are deposited on a moving filter. Next the air flows through the rotating filter stage C where particles smaller than 2.5 mm are deposited (http://www.pixeintl.com/Streaker.asp).

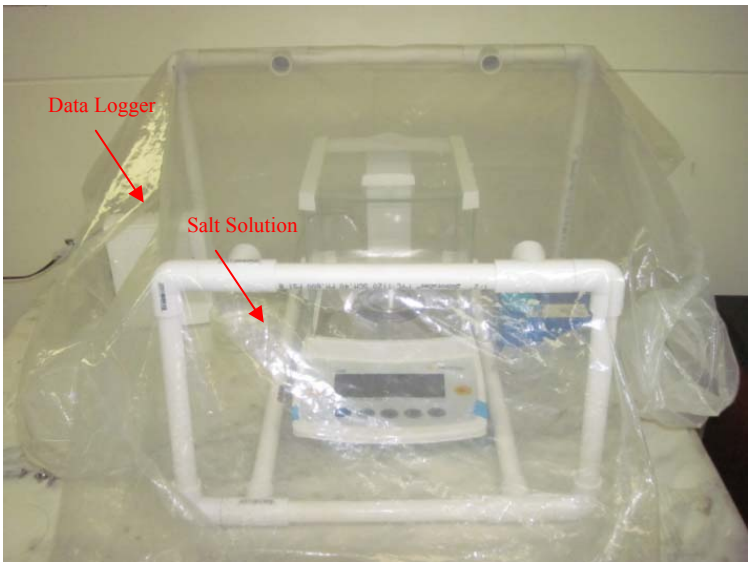

Figure 7: Pictures of Microbalance used to weigh the filters.

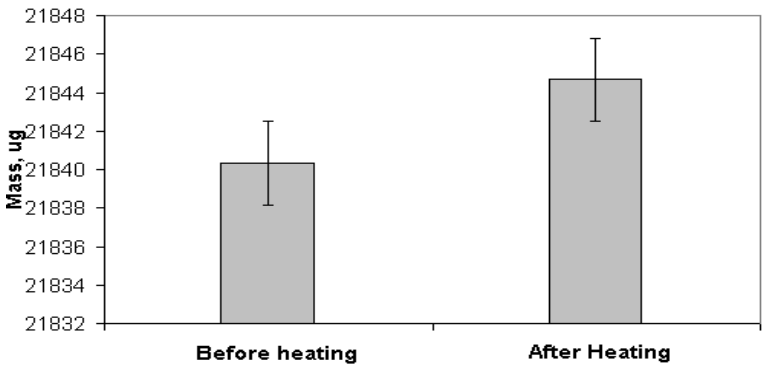

Figure 8: Weight difference of Al filters before and after heating test. Error bars show the standard error of measurement.

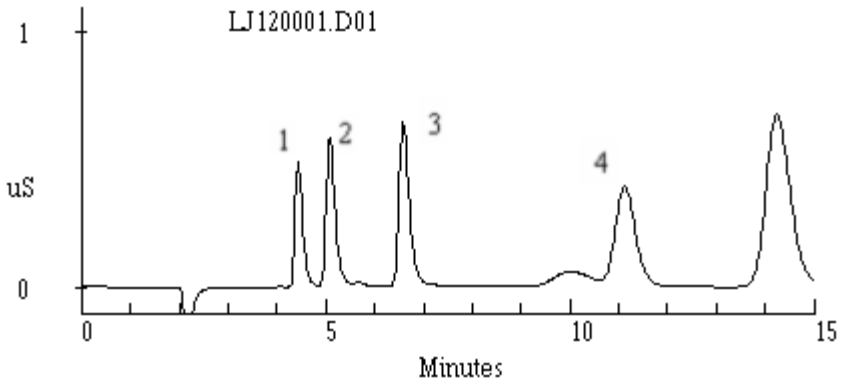

Figure 9: A sample chromatogram of cation analysis of sample collected from the downwind field site of West Texas. (1) Sodium;(2) Ammonium;(3) Potassium; (4) Calcium.

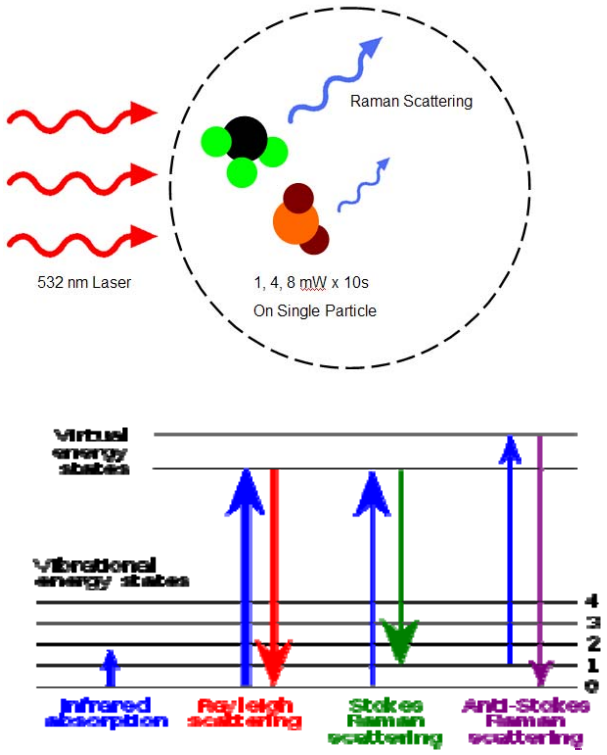

Figure 10: Concept of Raman MS's inelastic scattering.

(a)

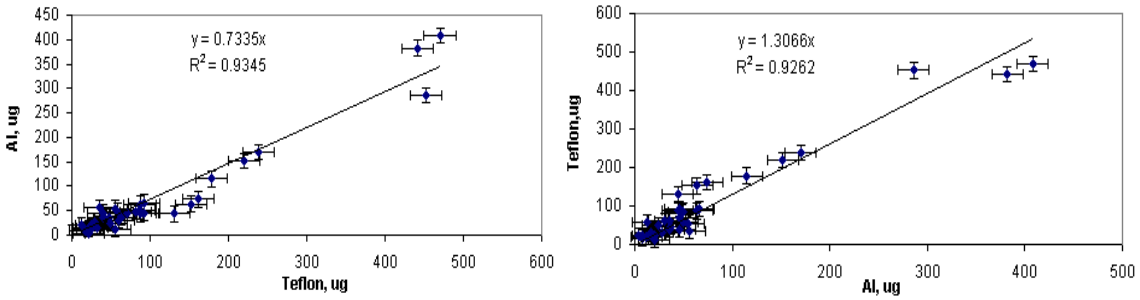

Geometric mean regression slope: 0.75

(b)

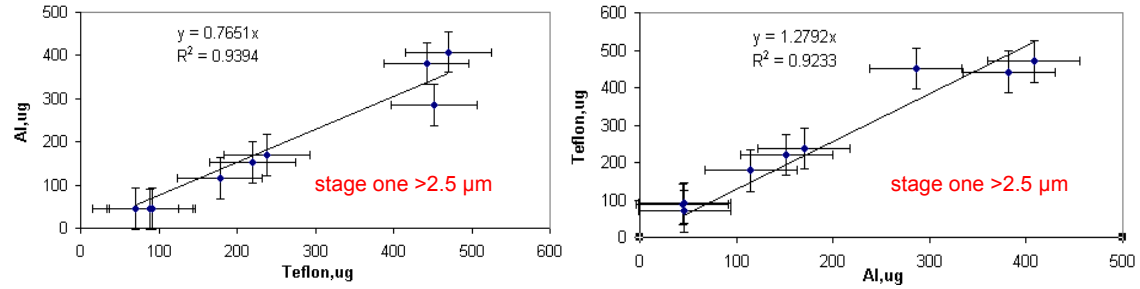

Geometric mean regression slope: 0.77

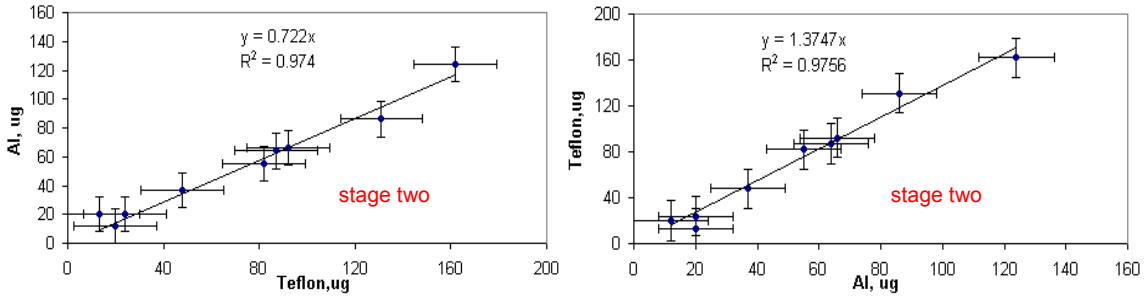

Geometric mean regression slope: 0.72

Figure 11: Total particle mass obtained by impactor samplers with Aluminum and Teflon filters. Total Particle mass obtained by impactor samplers with Aluminum and Teflon filters on each stage. The error bars represent the standard error for two different filters.

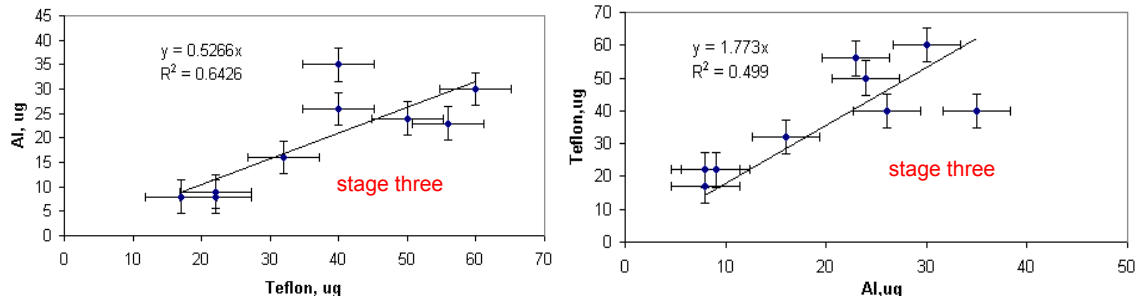

Geometric mean regression slope: 0.54

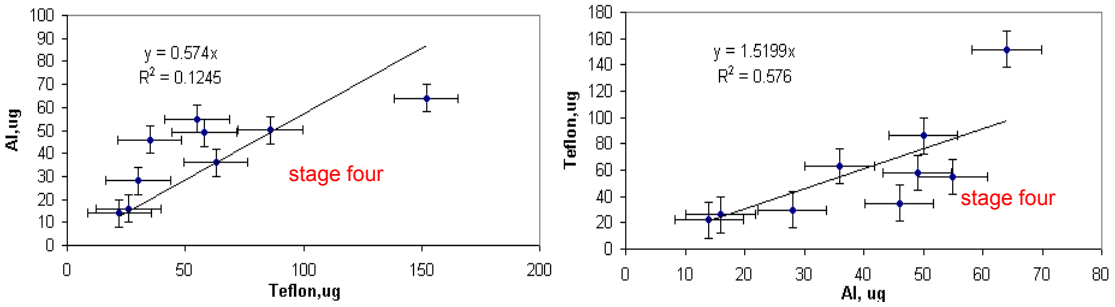

Geometric mean regression slope: 0.61

Figure 11 continued

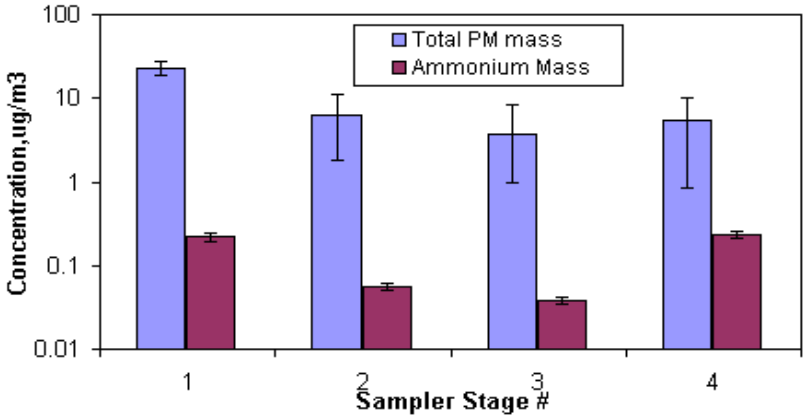

Figure 12: Average mass concentration of ammonium and particles at each stage of the sampler.

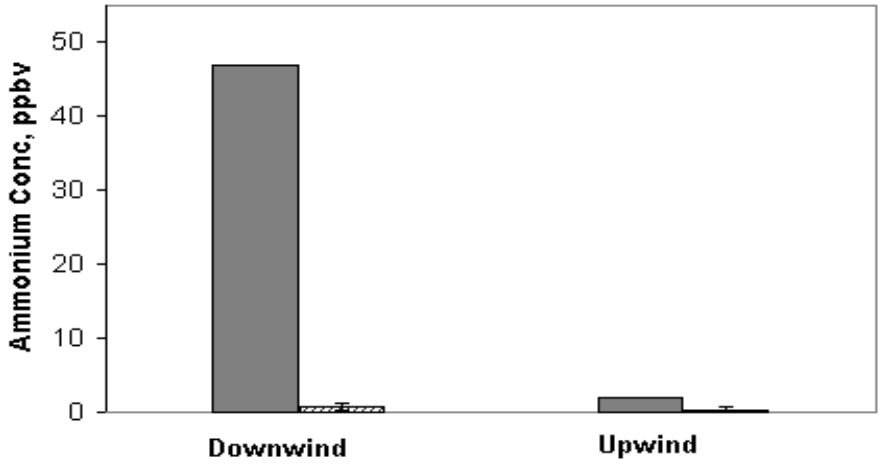

Figure 13: Average ammonia concentration from particulate matters sampled from downwind and upwind field sites. Total ammonia – gaseous ammonia (average difference, error is essentially 100%, aka within the detection limit) at downwind and upwind field sites dring the same time periods of 2007 (Hiranuma 2010).

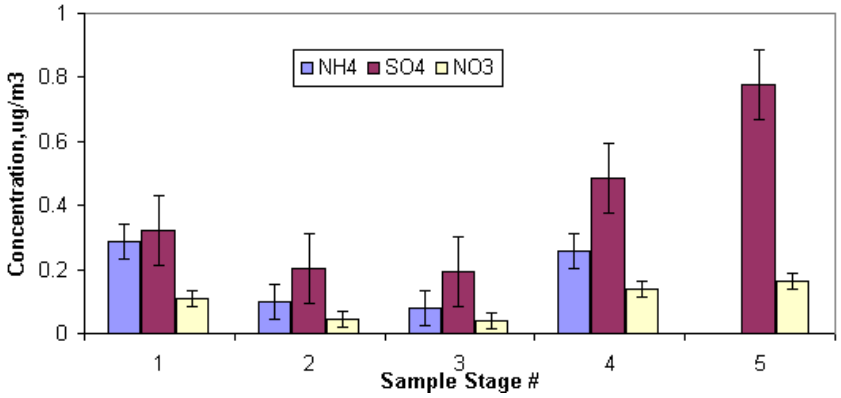

Figure 14: Average mass concentrations of ammonium, sulfate and nitrate at downwind site in West Texas. Error bars represent standard error from mean. No ammonium analyses were done on the back-up filter.

(a)

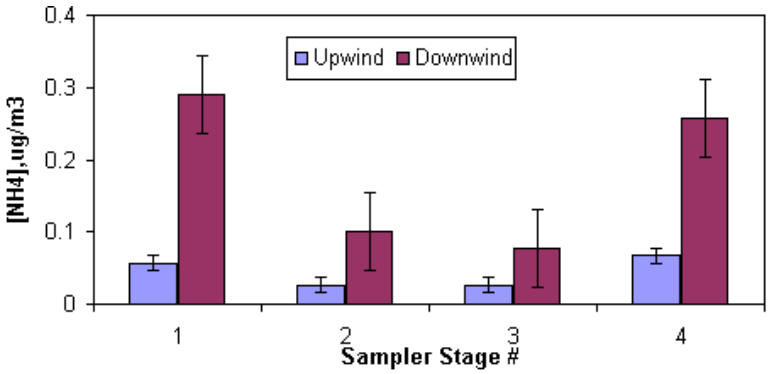

(b)

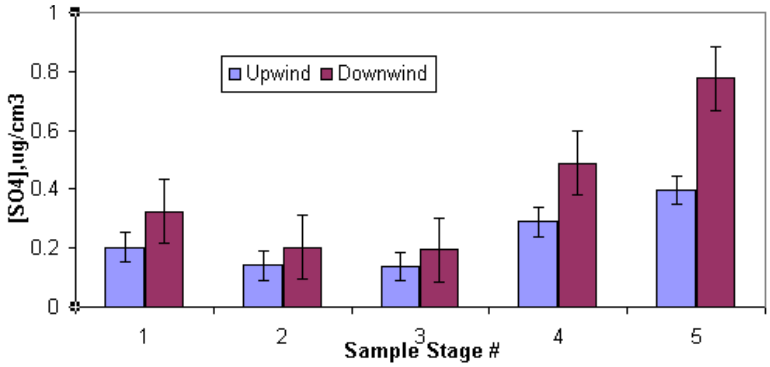

Figure 15: Average (a) ammonium and (b) sulfate mass concentrations sampled at upwind and downwind field sites. Error bars represent standard error from mean.

(a)

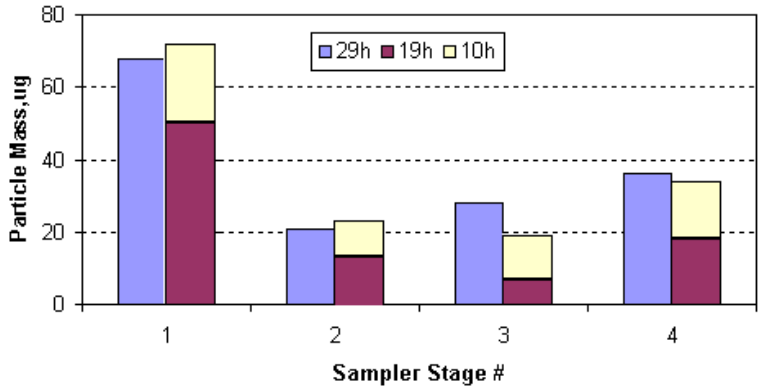

(b)

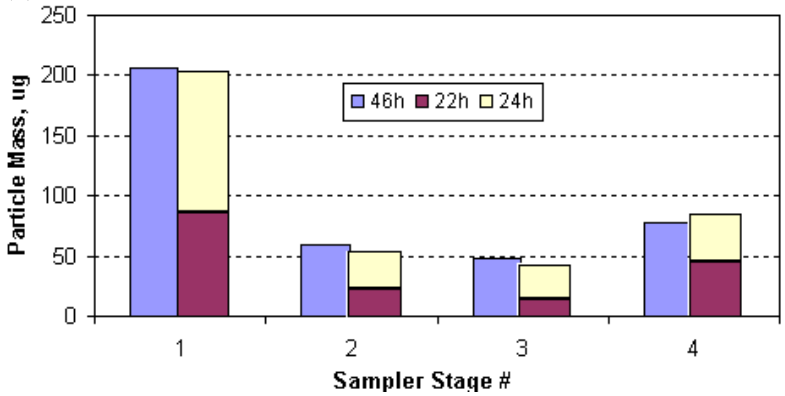

Figure 16: Particle mass obtained from different sample time. (a) Particle mass obtained from different sample time (29h, 19h and 10h separately) at Yellow cab; (b) Particle mass obtained from different sample time (46h, 22h and 24h separately) at Moody tower.

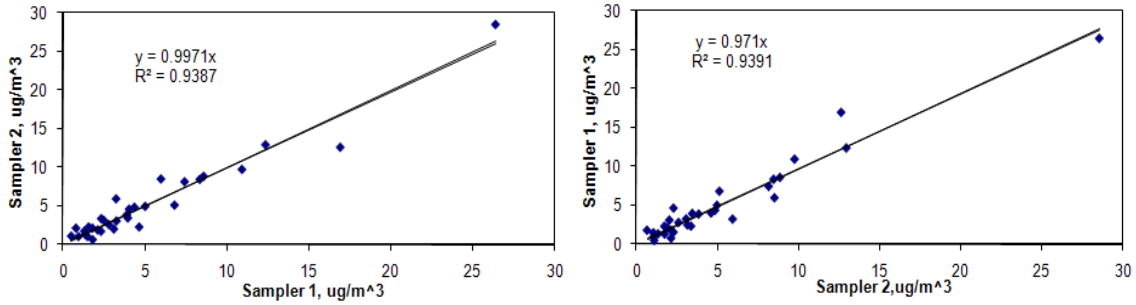

Geometric mean regression slope: 1.01

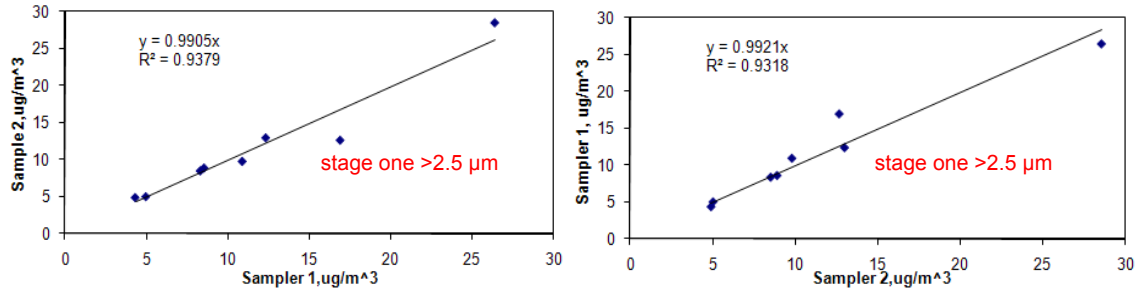

Geometric mean regression slope: 1.0

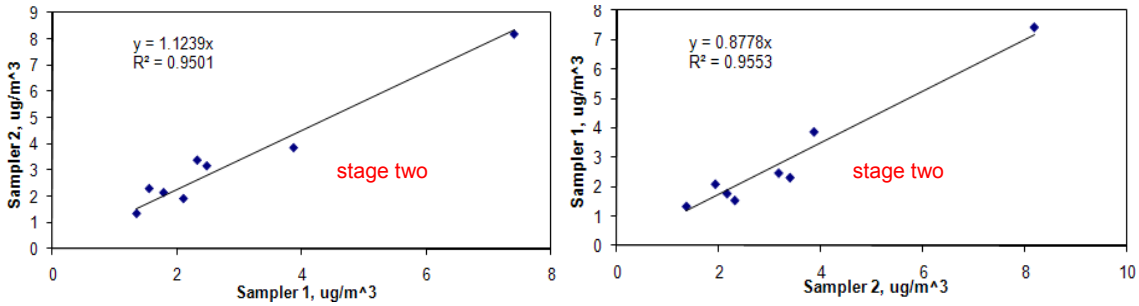

Geometric mean regression slope: 1.13

Figure 17: Total particle mass concentrations obtained by two samplers on four stages at Yellow Cab.

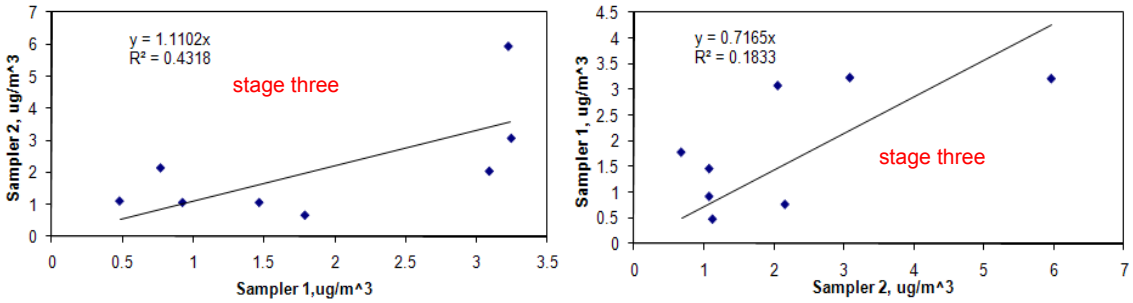

Geometric mean regression slope: 1.24

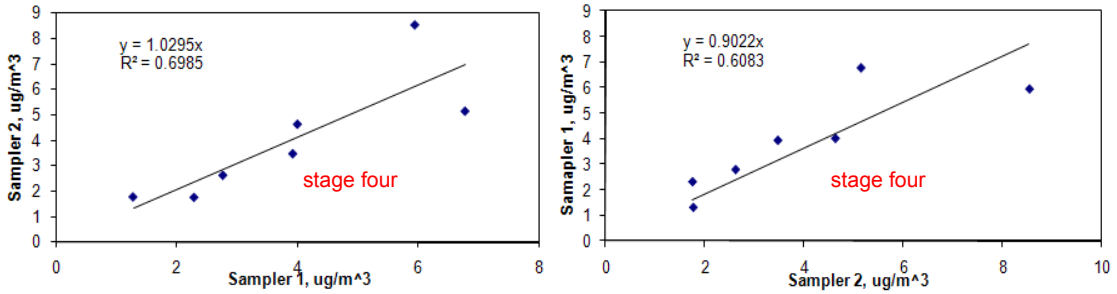

Geometric mean regression slope: 1.07

Figure 17 Continued

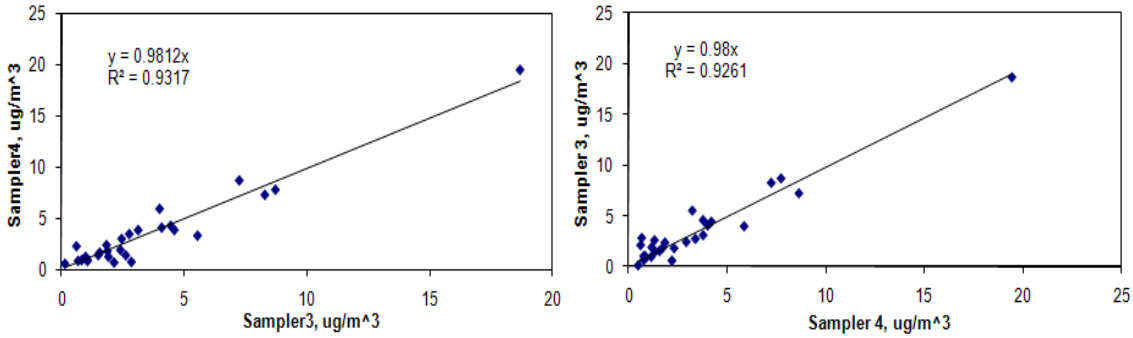

Geometric mean regression slope: 1.0

Figure 18: Total particle mass concentrations obtained by two samplers on four stages at Moody tower.

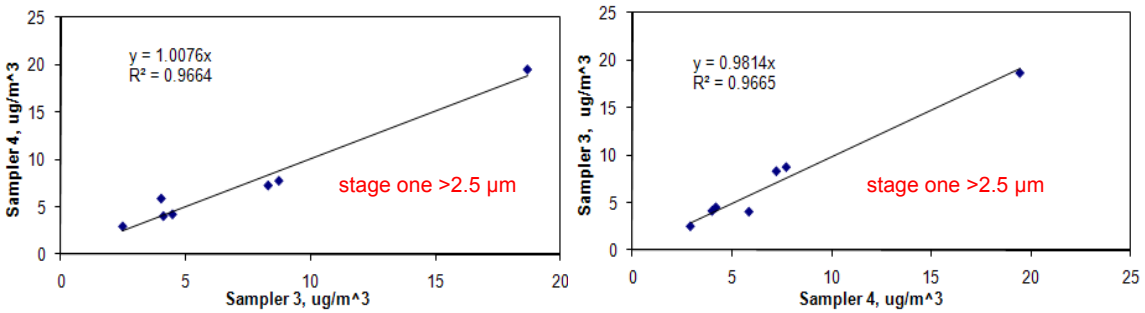

Geometric mean regression slope: 1.01

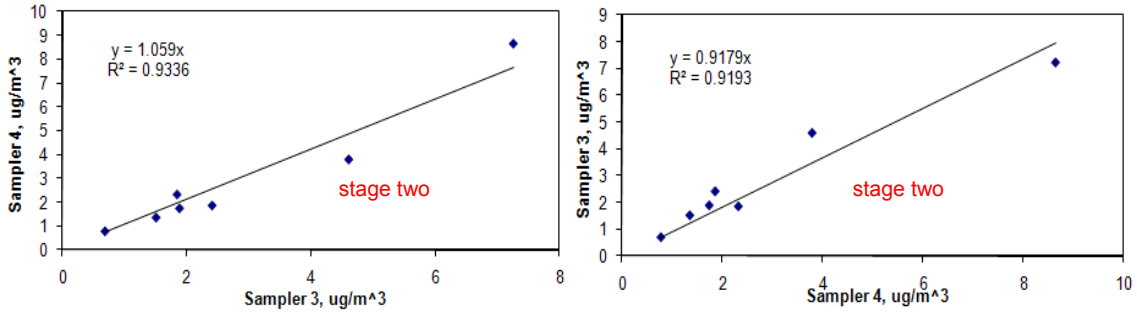

Geometric mean regression slope: 1.07

Figure 18 Continued

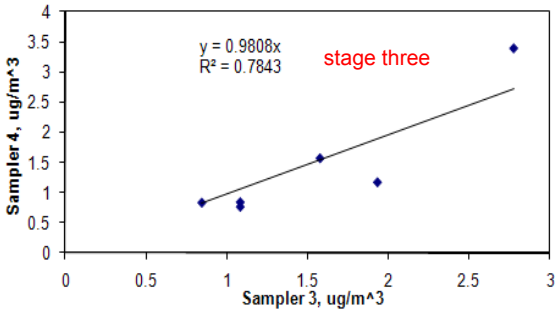

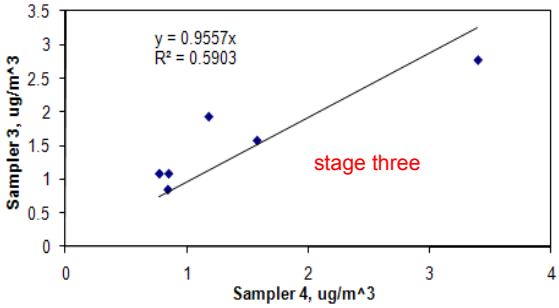

Geometric mean regression slope: 1.01

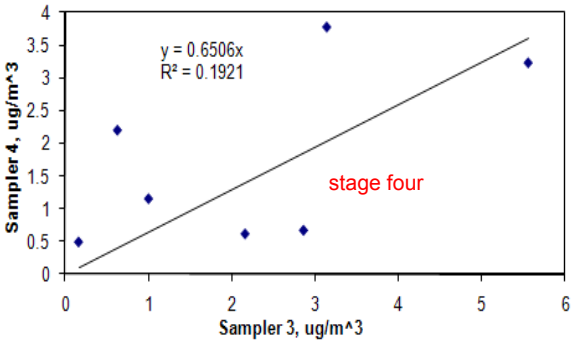

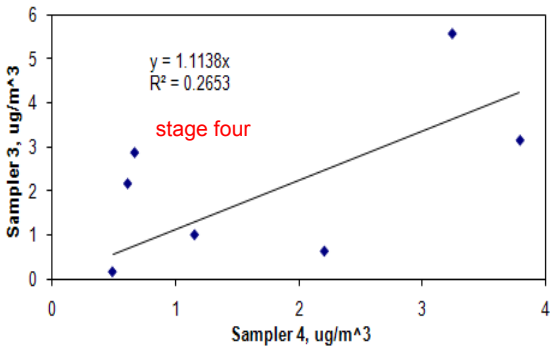

Geometric mean regression slope: 0.76

Figure 18 Continued

(a)

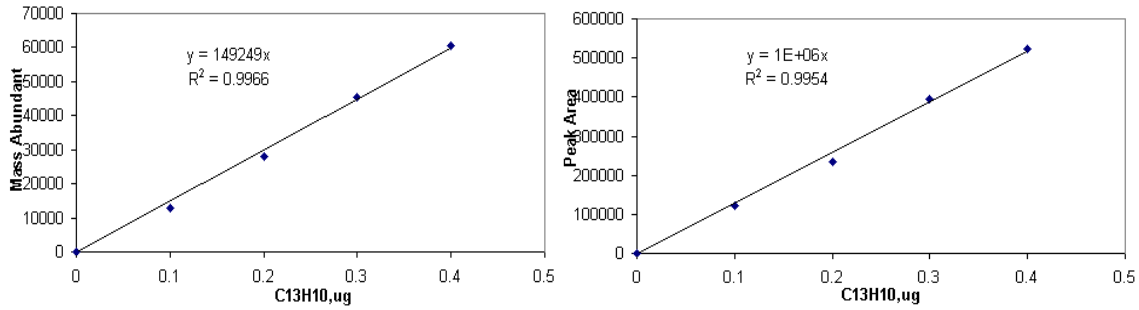

(b)

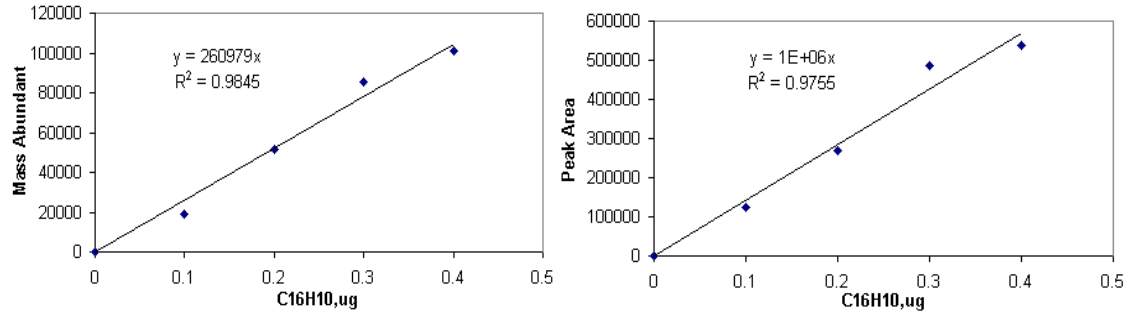

(c)

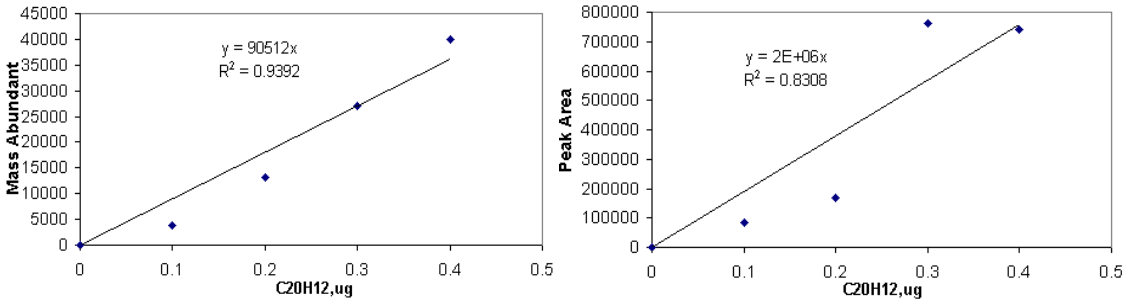

Figure 19: Three examples of a calibration curves. Linearity of PAH standard solution indicated by mass abundance (left) and peak areas (right) versus mass of PAH standard solutions injected on the filters, (a) Fluorene, (b) Pyrene, (c) Benzo(k)fluoranthene (c) Showed an example of a poor PAH calibration, with determination coefficients (R^2) of 0.94 for mass abundance and 0.83 for Peak area.

(a)

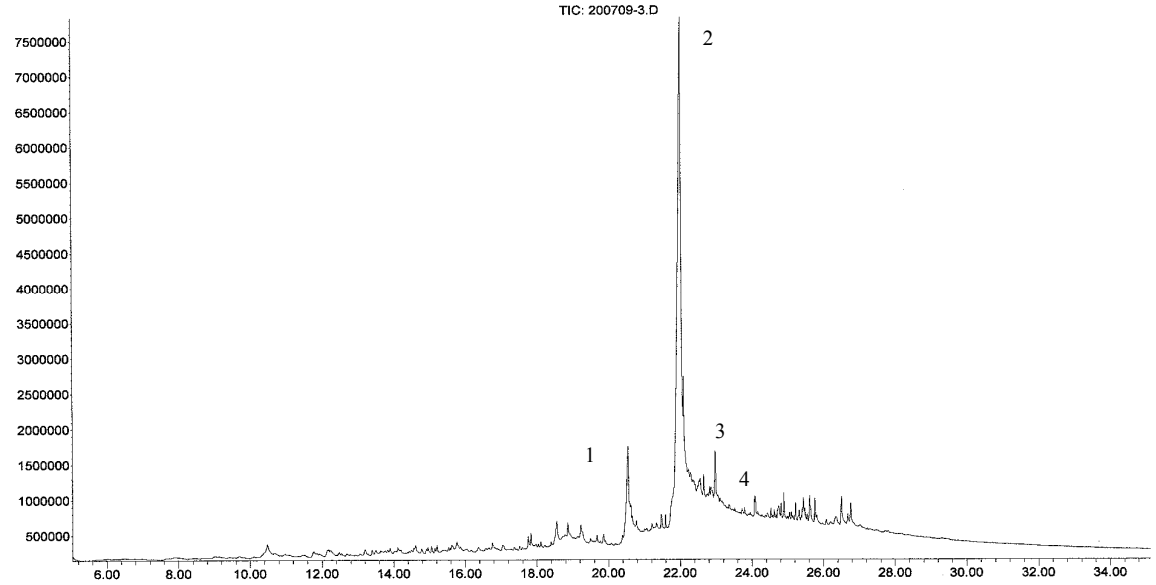

(b)

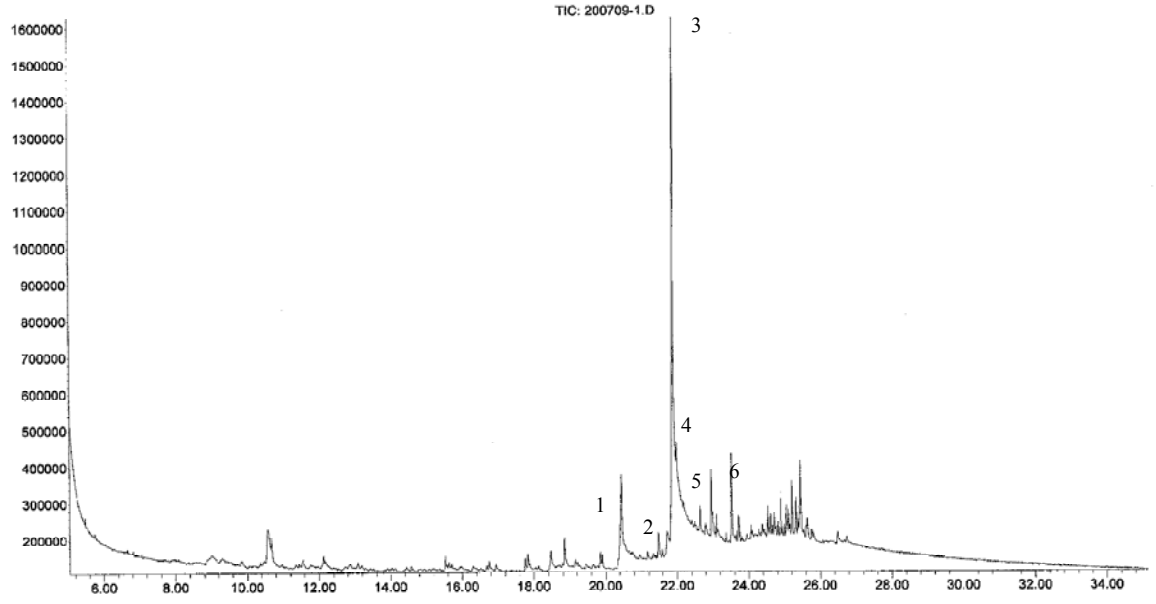

Figure 20: Total ion chromatograms of an aerosol filter sample from 2008 West Texas field measurement. (a). (1) n-Hexadecanoic acid; (2) Octadecanoic acid; (3) Hexadecanamide; (4) Teradecanamide; (b). (1) n-Hexadecanoic acid; (2) Haptadecanenitrile (3) Octadecanoic acid; (4) Hexadecanamide ;(5) Cyclotetracosane; (6) 1,2-Benzenedicarboxylic acid.

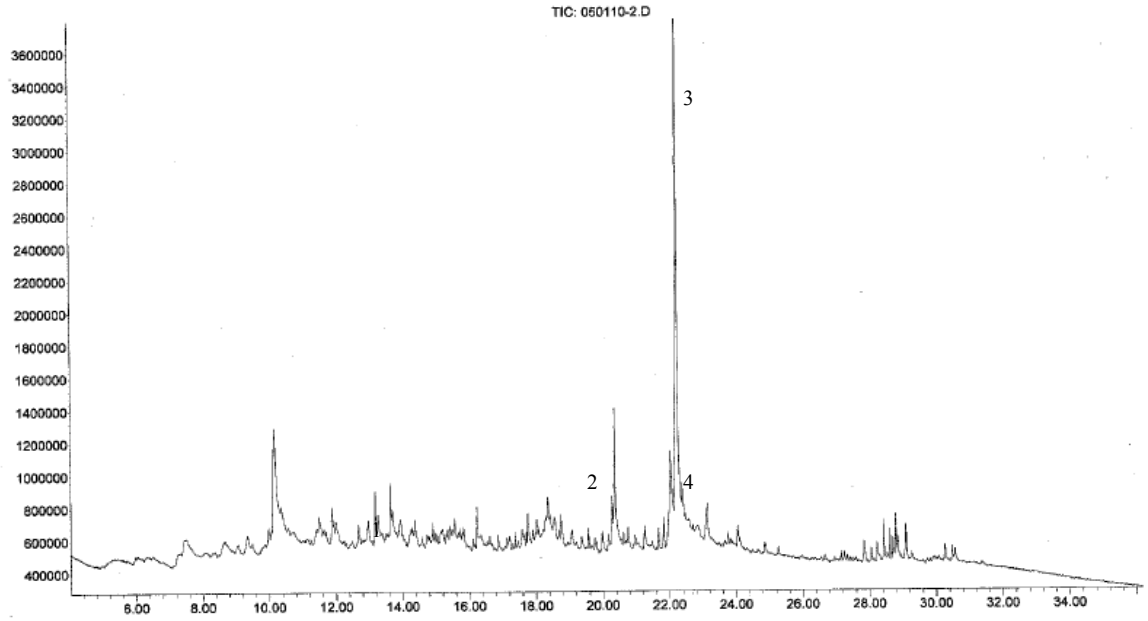

Figure 21 a: Example chromatograms of soil sample. Total ion chromatograms of ~500ug fine soil sample from West Texas field (1)2-Methoxy-4-vinylphenol; (2) n-Hexadecanoic acid; (3) Octadecanoic acid; (4) Hexadecanamide.

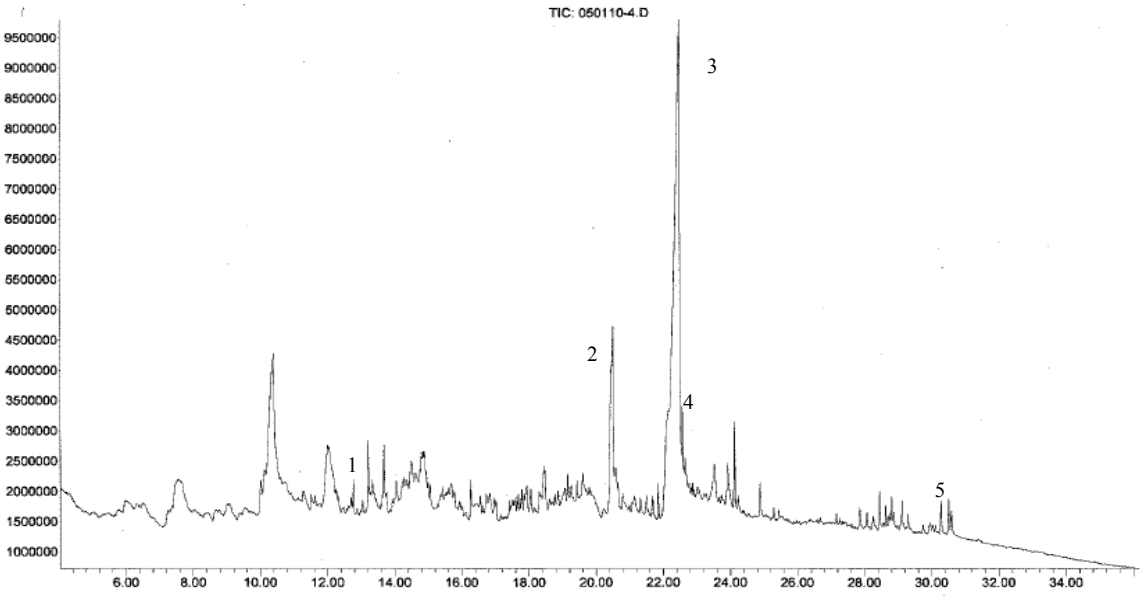

Figure 21 b: Example chromatograms of soil sample. Total ion chromatograms of ~726ug coarse soil sample from West Texas field. (1) 2-Methoxy-4-vinylphenol; (2) n-Hexadecanoic acid; (3) Octadecanoic acid; (4) Hexadecanamide; (5) Gamma Sitosterol.

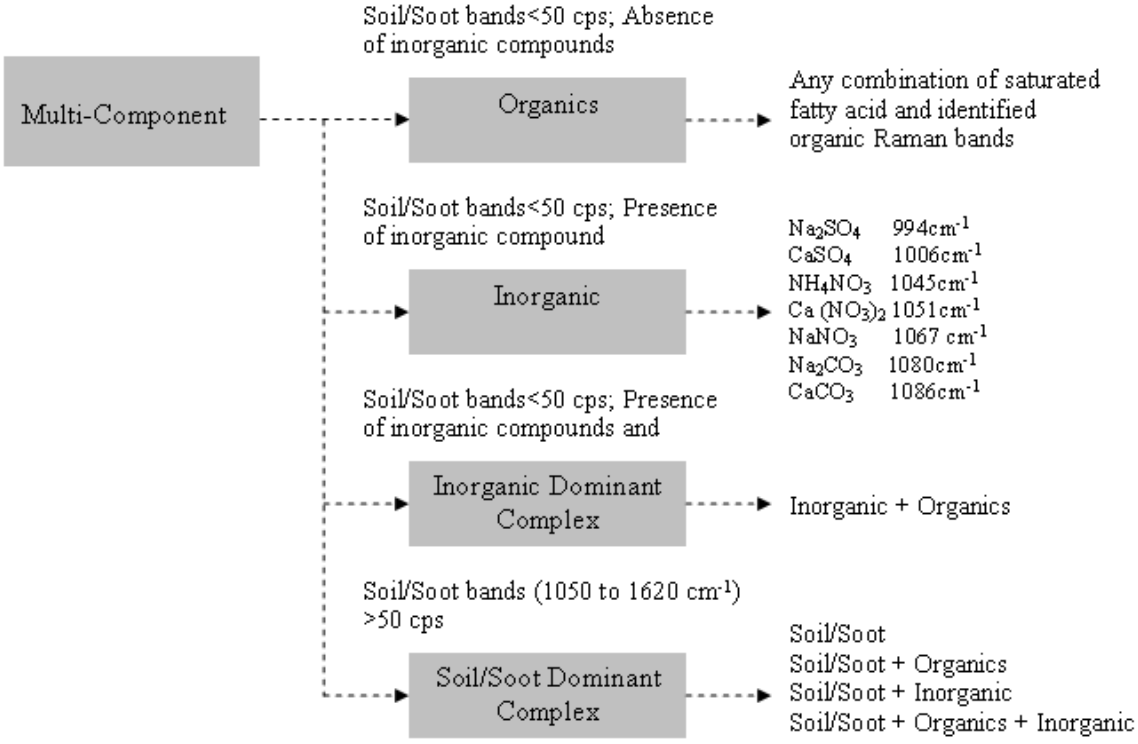

Figure 22: Qualitative classification of spectra types created by Raman mapping analysis of aerosols.

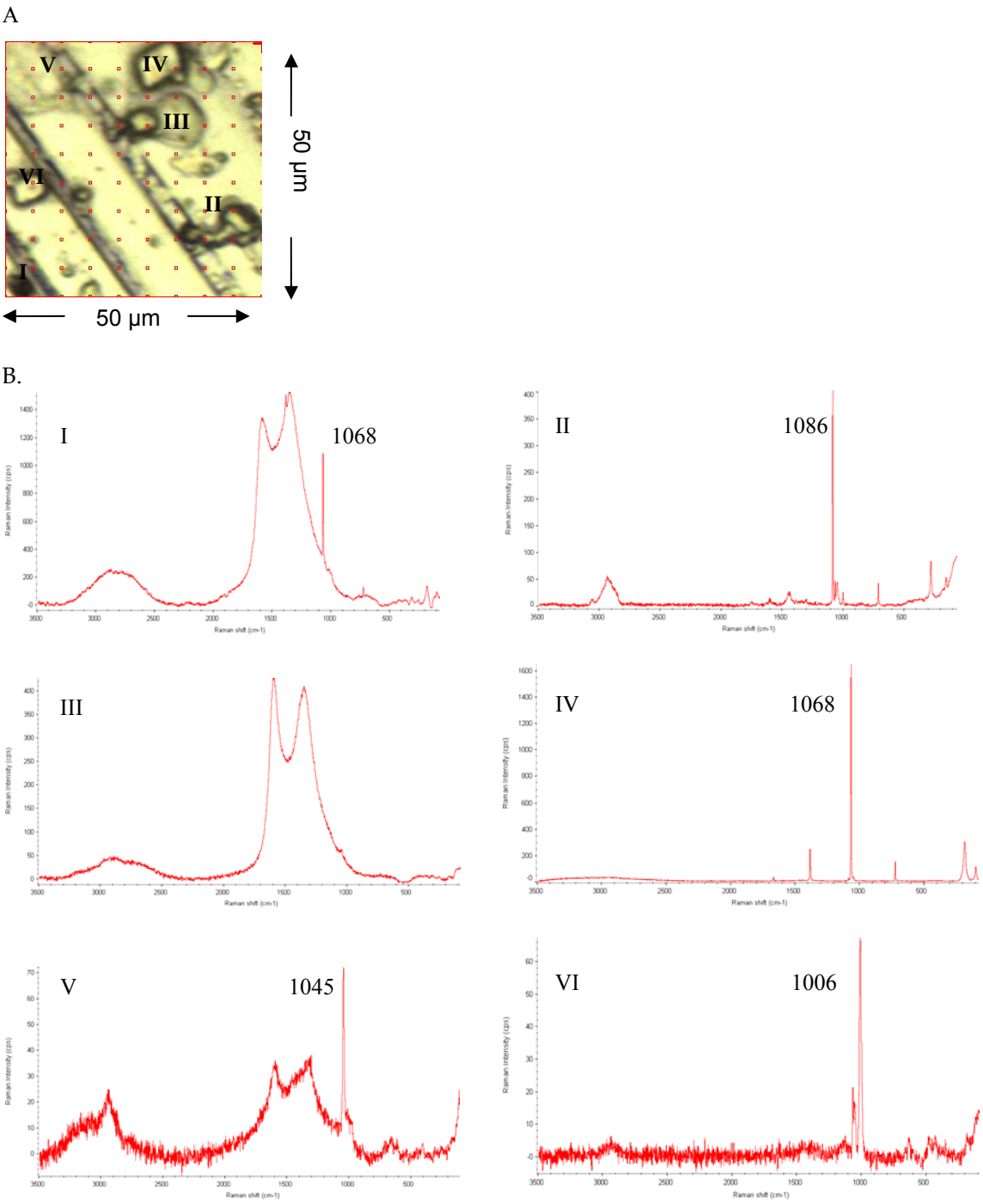

Figure 23: Representative Raman spectra of urban aerosols. (A) Microscopic image of particles derived from samples collected on Mar 21, 2009, at noon time. (B) Raman spectra of urban particle I, II, III, IV, V and VI in spectral range of 50 to 3500 cm^{-1}: (I) Soil/soot dominant complex with $NaNO_3$ at 1068 cm^{-1}, (II) $CaCO_3$ at 1086 cm^{-1}, (III) amorphous carbon with broad spectra ~1500 (1050-1620) cm^{-1}, (IV) $NaNO_3$ at 1068 cm^{-1}, (V) $NH4NO_3$ at 1045 cm^{-1}, (VI) $CaSO_4$ at 1006 cm^{-1}.

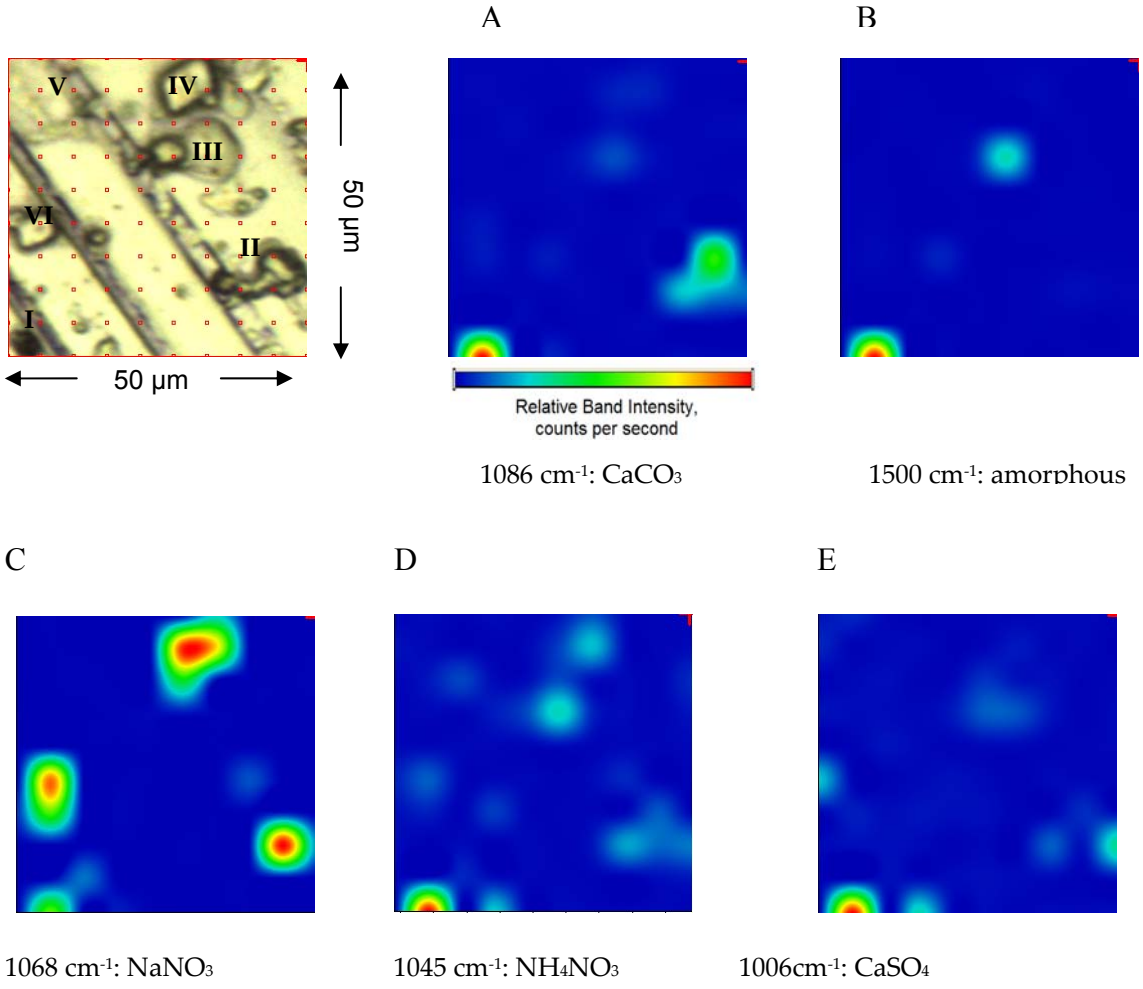

Figure 24: Chemical mapping by Raman microspectrometry. Chemical maps of selected molecular groups in aerosols at different Raman band position, (A) 1086 cm^{-1}: $CaCO_3$, (B) 1500 cm^{-1}: amorphous carbon, (C) 1068 cm^{-1} $NaNO_3$, (D) 1045 cm^{-1} $NH4NO_3$, (E) 1006 cm^{-1} $CaSO_4$. Mapping experiment was conducted on particles collected on March 21, 2009 at 11AM~12PM with a laser power of 8mW.

A

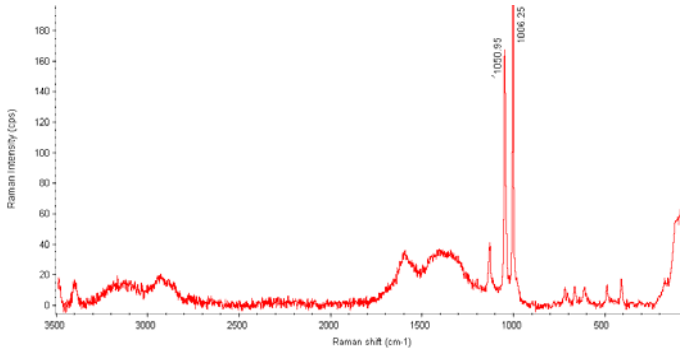

B

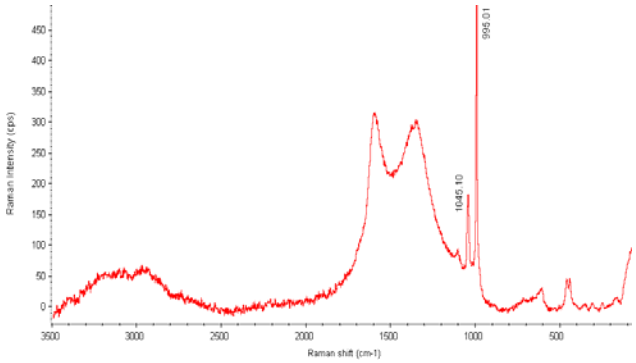

Figure 25: Qualitative classification of Raman spectra types. (A) inorganic dominant complex, (B) soil/soot dominant complex. Threshold is ≥50 cps. For these particular spectra, (A) 1006 cm^{-1} $CaSO_4$; 1050 cm^{-1} $Ca(NO_3)_2$, (B) 995 cm^{-1} Na_2SO_4; 1045 cm^{-1} NH_4NO_3; ~1500 HULIS bands. All spectra are measured on sample collected on March 21, 2009 at 6AM~9PM with a laser power of 8mW.

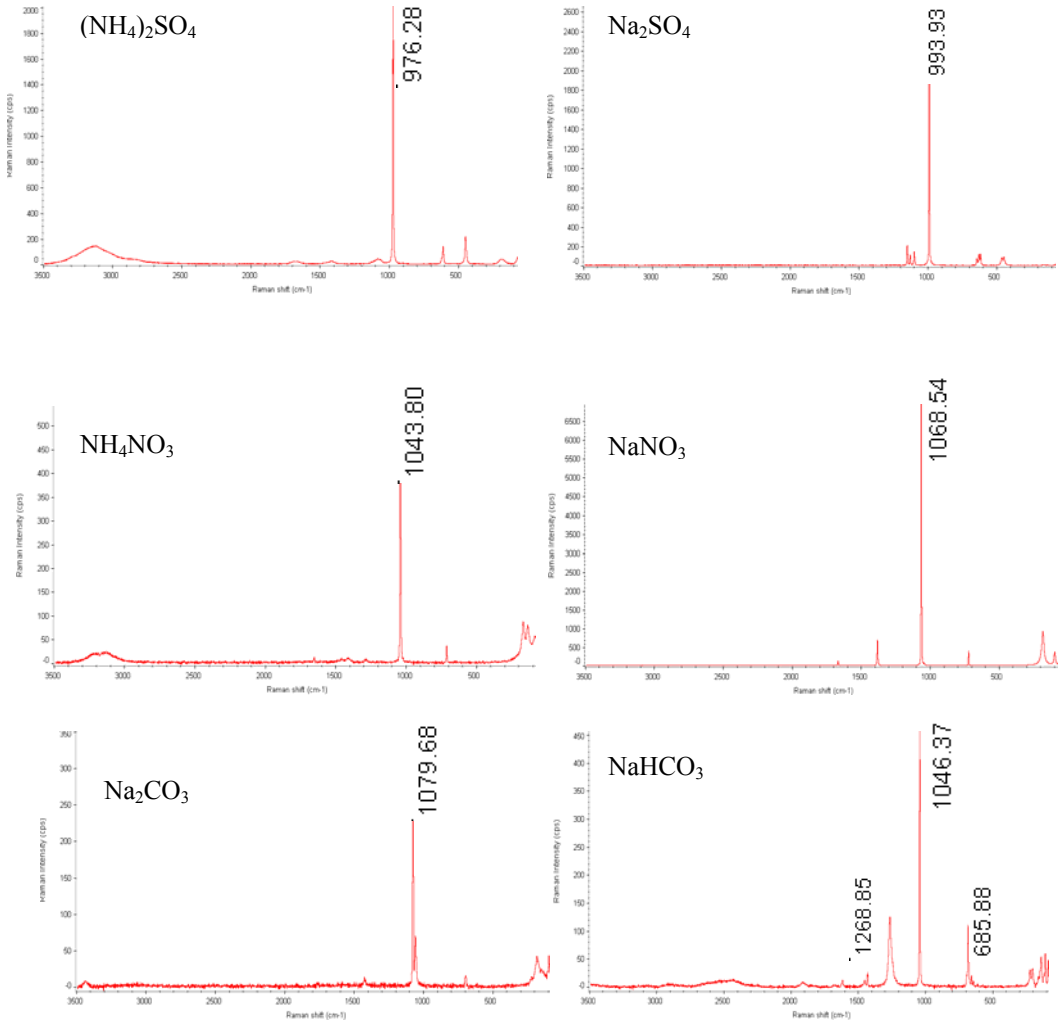

Figure 26: Raman spectra of salts, organics and HULIS found in atmospheric aerosols. Mapping experiment was conducted with a laser power of 4mW.

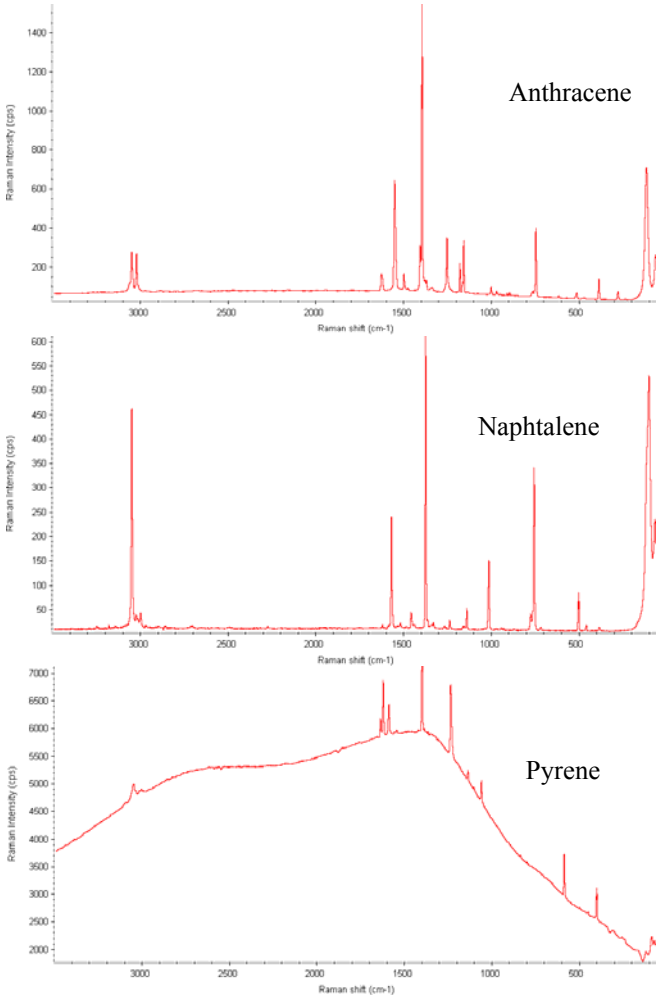

Figure 26 Continued

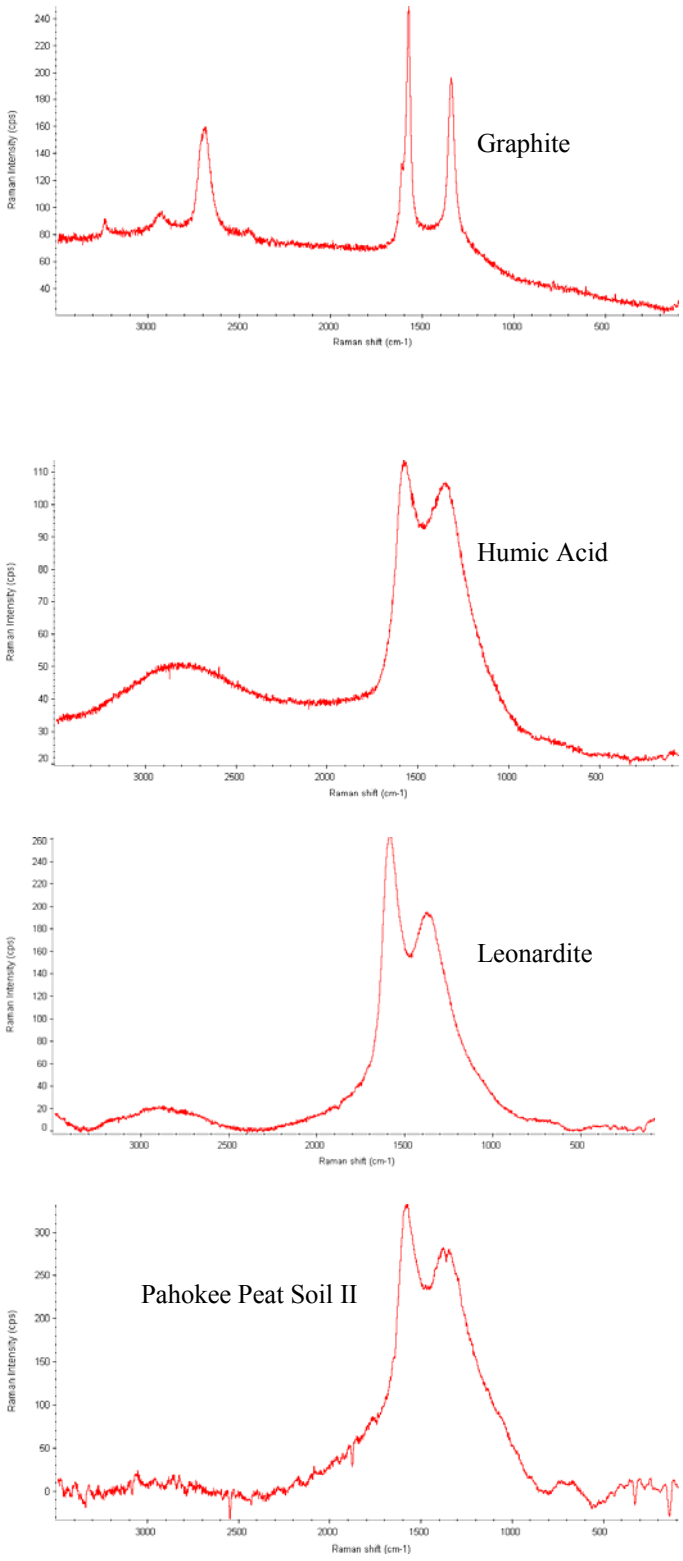

Figure 26 Continued

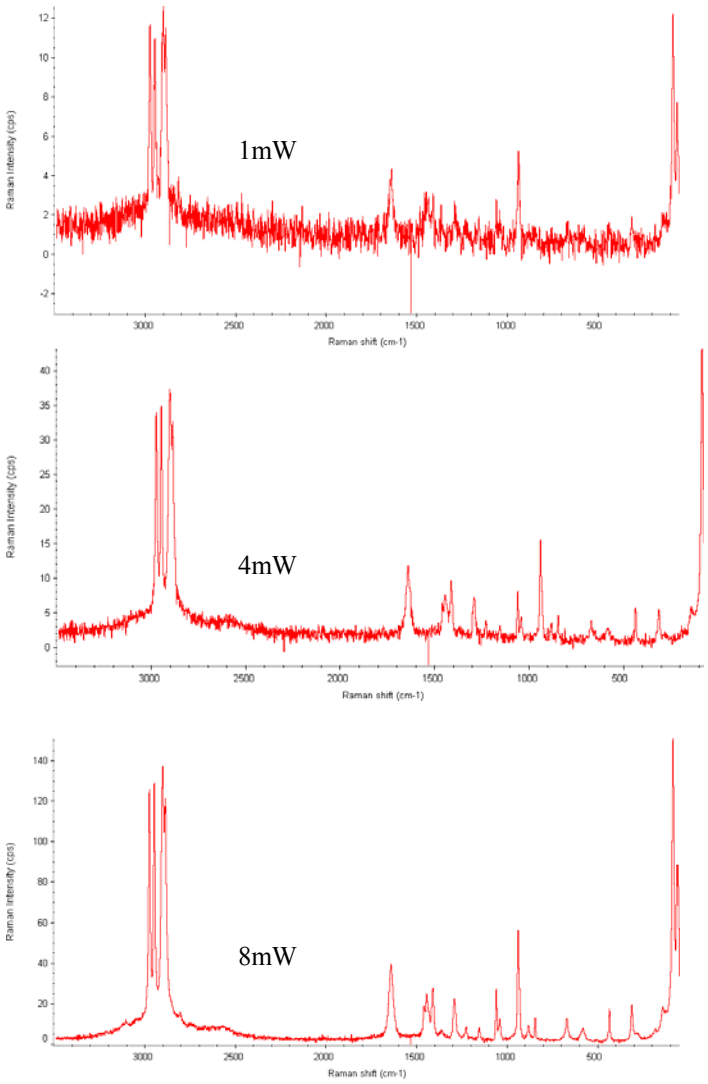

Figure 27: Roman spectra of Glutaric acid as function of laser intensity: 1mW, 4mW and 8mW.

Table 1. Physical properties, regression coefficients and retention time of n-alkanes and PAHs standards using in GC-MS/FID method.

n-Alkane	M.W	bp(°C)	R^2 /mass abundant	R^2 /peak area	t_R /min
n-Decane (C_{10})	174.2	174	0.9991	0.9998	7.78
n-Dodacane (C_{12})	316.3	216	0.9978	0.9626	11.54
n-Tetradecane (C_{14})	198.4	254	0.9901	0.8904	14.32
n-Hexadecane (C_{16})	226.4	287	0.9346	0.9844	16.69
n-Octadecane (C_{18})	254.5	316.1	0.9109	0.9998	18.81
n-Eicosane (C_{20})	282.6	342.7	0.9833	0.9968	20.76
n-Docosane (C_{22})	310.6	368.4	0.9944	0.9668	22.54
n-Tetracosane (C_{24})	338.7	391.3	0.9712	0.9999	24.16
n-Hexacosane (C_{26})	366.7	412.2	0.9935	0.9779	25.68
n-Octacosane (C_{28})	394.8	431.6	0.9712	0.9506	27.08
n-Triacosane (C_{30})	422.8	449.7	0.9581	0.9266	28.41
n-Dotracontane (C_{32})	450.9	467	0.9951	0.9559	29.64
n-Tetratriacontane(C_{34})	478.9	**	0.9823	0.9574	30.84
n-Hexatriacontane (C_{36})	507.0	**	**	**	**
n-Octatriacontane (C_{38})	535.0	**	**	**	**
n-Tetracontane (C_{40})	563.1	**	**	**	**

PAH	M.W	bp(°C)	R^2/mass abundante	R^2/peak area	t_R /min
Naphthalene	128.2	218	0.9965	0.9938	11.27
Acenaphthylene	152.2	265	0.9786	0.9711	15.05
Acenapthene	154.2	279	0.9989	0.9929	15.46
Fluorene	166.2	295	0.9641	0.9978	16.67
Phenanthrene	178.2	340	0.8866	0.9862	18.84
Anthracene	178.2	340	0.9823	0.9778	18.96
Fluoranthene	202.3	375	0.9859	0.9384	21.55
Pyrene	202.3	404	0.9774	0.9537	22.06
Benz[a]anthracne	228.3	437.6	0.9554	0.9338	24.85
Chrysene	228.3	448	0.9816	0.9249	24.93
Benzo[b]fluoranthene	252.3	357	0.9818	0.9614	27.17
Benzo[k]fluoranthene	252.3	480	0.9934	0.8351	27.23
Benzo[a]pyrene	252.3	495	0.9449	0.8941	27.79
Indeno[1,2,3-cd]pyrene	276.3	536	***	***	29.83
Dibenz[a,h]anthracne	278.4	524	***	***	30.25
Benzo[g,h,i]perylene	276.3	500	***	***	***

Table 2. Ordinary least squares (OLS) regression Coefficient and Geometric Mean of two slopes. (a) for Yellow Cab samples; (b) for Moody Tower samples.

(a)

	OLS(Y on X)	OLS(X on Y)	GMR	R^2
Total	0.979	0.9595	1.01011	0.9394
Stage A	1.0144	0.9252	1.047097	0.9386
Stage B	1.0476	0.9138	1.070711	0.9573
Stage C	0.9904	0.4447	1.492354	0.4404
Stage D	1.0177	0.6865	1.217558	0.6986

(b)

	OLS(Y on X)	OLS(X on Y)	GMR	R^2
Total	1.0051	0.9281	1.040656	0.9328
Stage A	0.9946	0.9718	1.011663	0.9666
Stage B	1.15	0.8197	1.184463	0.9427
Stage C	1.278	0.6556	1.396195	0.5625
Stage D	0.4268	0.8034	0.728864	0.3429

Table 3. Identified compounds collected from West Texas field site and possible quantification for dominant organic compounds. “na” denote “not available”, relative mass of total observable organics are calculated by integration of total FID area counts.

Compound	Formula	MW	Correction Factors	Mass,ng	Relative Mass, %
Tetradecanoic acid	$C_{14}H_{28}O_2$	228	1.15	113	0.2
Hexadecanoic acid	$C_{16}H_{32}O_2$	256	1.15	154	0.5
Octadecanoic acid	$C_{18}H_{36}O_2$	284	1.12	314	1.4
Tetradecanamide	$C_{14}H_{29}NO$	227	1.15	na	na
Hexadecanamide	$C_{16}H_{33}NO$	255	1.13	na	na
Cyclotetracosane	$C_{24}H_{48}$	337	0.99	na	na
Cholesterol	$C_{27}H_{46}O$	387	1.01	na	na
Total Observable Organics	na	na	1.00	na	5.6

Table 4. Raman frequencies observed in spectra of agricultural aerosols and their tentative assignments to the classes of vibrational modes.

Raman Shift, cm-1	Tentative Assignment [a,b,c]
Chemical bonding of Organics (<525/>2700 cm^{-1})	
178 cm^{-1}	symmetric CI_4 stretches
160 to 200 cm^{-1}	skeletal deformation of aliphatic nitriles
267 cm^{-1}	symmetric CBr_4 stretch in solution
335 to 355 cm^{-1}	skeletal deformation of monoalkyl acetylenes
150 to 425 cm^{-1}	chain expansion of n-alkanes
437 cm^{-1}	symmetric CI_3 stretch of CHI_3 (in solution)
459 cm^{-1}	symmetric CCl_4 stretch
483 cm^{-1}	symmetric CI_2 stretch
484 to 475 cm^{-1}	skeletal deformation of dialkyl diacetylenes
485 to 495 cm^{-1}	CI stretch of secondary/tertiary iodoalkanes
480 to 510 cm^{-1}	SS stretches of dialkyl trisulfides
500 to 510 cm^{-1}	CI stretch of primary iodoalkanes
523 cm^{-1}	CI stretches from CH_3I
510 to 525 cm^{-1}	SS stretch of dialkyl disulfides
2700 to 2850 cm^{-1}	CHO group vibration of aliphatic aldehydes
2849 to 2969 cm^{-1}	symmetric/antisymmetric stretches of n-alkanes ($-CH_2$/$-CH_3$)
2986 to 2974 cm^{-1}	symmetric NH_3^+ stretch of aqueous alkyl ammonium chlorides
2980 to 2990 cm^{-1}	symmetric $=CH_2$ stretches of $C=CH_2$ derivatives
3026 cm^{-1}	symmetric $=CH_2$ stretches of ethylene (gas)
3000 to 3040 cm^{-1}	CH stretch of C=CHR derivatives
3057 cm^{-1}	aromatic CH stretch of alkyl benzenes
3062 cm^{-1}	CH stretch of benzene
3070 to 3095 cm^{-1}	antisymmetric $=CH_2$ stretch of $C=CH_2$ derivatives
3000 to 3100 cm^{-1}	aromatic CH stretch of benzene derivatives
3020 to 3100 cm^{-1}	CH_2 stretches of cyclopropane
3103 cm^{-1}	antisymmetric $=CH_2$ stretch of ethylene (gas)
3154 to 3175 cm^{-1}	bonded NH stretch of pyrazoles
3145 to 3190 cm^{-1}	bonded symmetric NH_2 stretch of primary amides
3290 to 3310 cm^{-1}	bonded NH stretch of secondary amides
3250 to 3300 cm^{-1}	bonded symmetric NH_2 stretch of primary amines
3300 to 3350 cm^{-1}	$\equiv$CH stretch of alkyl acetylenes
3325 to 3355 cm^{-1}	bonded antisymmetric NH_2 stretch of primary amines
3374 cm^{-1}	CH stretch of acetylene (gas)
3340 to 3380 cm^{-1}	bonded OH stretch of aliphatic alcohols
3330 to 3400 cm^{-1}	bonded antisymmetrc NH_2 stretch of primary amines
Inorganics (Major Peak)	
976 cm^{-1}	ammonium sulfate ($(NH_4)_2SO_4$)
994 cm^{-1}	sodium sulfate (Na_2SO_4)
1006 cm^{-1}	calcium sulfate ($CaSO_4$)
1044 cm^{-1}	ammonium nitrate (NH_4NO_3)
1046 cm^{-1}	bi-sodium carbonate ($NaHCO_3$)
1050 cm^{-1}	calcium nitrate ($Ca(NO_3)_2$)
1069 cm^{-1}	sodium nitrate ($NaNO_3$)
1080 cm^{-1}	sodium carbonate (Na_2CO_3)
1088 cm^{-1}	calcium carbonate ($CaCO_3$)

Table 4 Continued

Raman Shift, cm-1	Tentative Assignment [a,b,c]
Inorganics (Minor Peaks)	
452/615/2263/3122 cm^{-1}	$(NH_4)_2SO_4$
450/621/1102-1153 cm^{-1}	Na_2SO_4
414/493/619/700/1134 cm^{-1}	$CaSO_4$
140-172/715/832/1385/1768/ 2399/3023-3133 cm^{-1}	NH_4NO_3
112-207/686/1269/1433 cm^{-1}	$NaHCO_3$
187/725/1386 cm^{-1}	$NaNO_3$
187/699/1062 cm^{-1}	Na_2CO_3
280/712 cm^{-1}	$CaCO_3$

[a,b] Organic chemical bond on the basis of Dollish et al. (1974) and Schulte et al. (2008)
[c] For identification of Raman spectra (band wavenumbers and relative intensities) of inorganics, the resolved spectra are compared with commercially available spectral libraries (Thermo Scientific, Nicolet Instruments, Marcel Dekker Inc.).

Table 5. Chemical composition of aerosols measured by Raman at different laser intensity. Aerosols obtained in morning March 21, 2009 at 1mW, 4mW, 8mW: investigated area, number of particle deposition spots investigated; ratio of the number of all spectra with signals characteristic for each component ± standard errors from averaging over different particle deposition spots.

	1mW		4mw		8mW	
	AVG	STDERROR	AVG	STDERROR	AVG	STDERROR
Investigated Area, µm x µm	50 x 50		50 x 50		50 x 50	
Investigated Spots	3		3		3	
Recorded specra	48.00		137.00		176.00	
Characteric spectra, %	100.00	0.00	100.00	0.00	100.00	0.00
High fluorescence, %	0.00	0.00	0.00	0.00	0.00	0.00
Organics(<525cm-1,> 2700cm-1),%	1.33	0.33	7.43	0.35	13.45	0.62
Inorganics,%	16.75	1.93	10.19	0.62	3.57	0.27
Na_2SO_4, %, ~994 cm^{-1}	0.00	0.00	1.71	0.25	0.00	0.00
$CaSO_4$, %, ~1006cm^{-1}	11.42	0.64	3.83	0.29	2.02	0.16
NH_4NO_3, %,~1045cm^{-1}	0.00	0.00	1.06	0.16	1.07	0.07
$Ca(NO_3)_2$, %,~1051cm^{-1}	5.33	1.33	3.60	0.34	0.48	0.06
$NaNO_3$, %, ~1067cm^{-1}	0.00	0.00	0.00	0.00	0.00	0.00
Na_2CO_3, %,~1080cm^{-1}	0.00	0.00	0.00	0.00	0.00	0.00
$CaCO_3$, %, ~1086cm^{-1}	0.00	0.00	0.00	0.00	0.00	0.00
Inorganic Dominant Complex, %	5.33	1.33	9.86	0.47	7.60	0.25
$NaNO_3$+$CaCO_3$	0.00	0.00	0.00	0.00	0.00	0.00
NH_4NO_3+$CaSO_4$	1.33	0.33	5.20	0.04	2.40	0.11
NH_4NO_3+Na_2SO_4	0.00	0.00	0.00	0.00	0.60	0.08
$Ca(NO_3)_2$+NaNO3	0.00	0.00	0.00	0.00	0.00	0.00
$Ca(NO_3)_2$+Na_2SO_4	0.00	0.00	0.00	0.00	0.00	0.00
$Ca(NO_3)_2$+$CaSO_4$	2.67	0.67	2.01	0.15	0.67	0.09
$Ca(NO_3)_2$+$CaCO_3$	0.00	0.00	0.00	0.00	0.00	0.00
$NaNO_3$+ $CaSO_4$	0.00	0.00	0.00	0.00	0.00	0.00
$NaNO_3$+ Other organics	0.00	0.00	0.00	0.00	0.00	0.00
NH_4NO_3+ Other organics	0.00	0.00	0.53	0.08	0.48	0.06
$Ca(NO_3)_2$+Other organics	1.33	0.33	1.59	0.23	1.43	0.19
NH_4NO_3+$CaSO_4$+other organics	0.00	0.00	0.00	0.00	0.60	0.08
$Ca(NO_3)_2$+$CaSO_4$+other organics	0.00	0.00	0.53	0.08	1.43	0.19
Soil/Soot Dominant Complex,%	76.58	3.58	72.52	0.67	74.79	0.16
Soil/Soot	72.87	3.62	56.52	1.83	48.86	1.14
Soil/Soot+ NH_4NO_3	1.33	0.33	4.35	0.14	3.79	0.25
Soil/Soot+ $NaNO_3$	0.00	0.00	0.00	0.00	0.00	0.00
Soil/Soot+ $CaSO_4$	2.38	0.60	0.00	0.00	2.10	0.16
Soil/Soot+ $CaCO_3$	0.00	0.00	0.00	0.00	0.00	0.00
Soil/Soot+ $Ca(NO_3)_2$	0.00	0.00	3.17	0.47	3.81	0.50
Soil/Soot+ $CaCO_3$+$NaNO_3$	0.00	0.00	0.00	0.00	0.00	0.00
Soil/Soot+ $Ca(NO_3)_2$+$CaSO_4$	0.00	0.00	1.59	0.23	0.95	0.12
Soil/Soot+ $Ca(NO_3)_2$+$CaCO_3$	0.00	0.00	0.00	0.00	0.00	0.00
Soil/Soot+ NH_4NO_3+$CaSO_4$	0.00	0.00	3.39	0.10	4.24	0.20
Soil/Soot+ NH_4NO_3+$NaNO_3$	0.00	0.00	0.00	0.00	0.00	0.00
Soil/Soot+ NH_4NO_3+Na_2SO_4	0.00	0.00	0.85	0.13	1.19	0.16
Soil/Soot+ $Ca(NO_3)_2$+Other organics	0.00	0.00	2.12	0.31	5.43	0.58
Soil/Soot+ NH_4NO_3+Other organics	0.00	0.00	0.00	0.00	3.55	0.17
Soil/Soot+Other organics	0.00	0.00	0.53	0.08	0.60	0.08

Table 6. Chemical composition of aerosols measured by Raman at different sampling time. Aerosols obtained at midnight, morning and noon time March 21, 2009: investigated area, number of particle deposition spots investigated; number of spectra recorded; ratio of the number of all spectra with signals characteristic for each component ± standard errors from averaging over different particle deposition spots.

	MIDNIGHT		MORNING		NOON	
	AVG	STDERROR	AVG	STDERROR	AVG	STDERROR
Investigated Area, μm x μm	50x50		50x50		50x50	
Investigated Spots	3		3		3	
Recorded specra	134.00		176.00		99.00	
Characteric spectra, %	97.44	0.23	100.00	0.00	100.00	0.00
High fluorescence, %	2.56	0.23	0.00	0.00	0.00	0.00
Organics(<525cm-1,> 2700cm-1),%	12.31	0.65	13.45	0.62	23.22	0.33
Inorganics,%	11.34	0.86	3.57	0.27	28.13	1.93
Na_2SO_4, %, ~994 cm^{-1}	0.00	0.00	0.00	0.00	0.00	0.00
$CaSO_4$, %, ~1006 cm^{-1}	2.16	0.17	2.02	0.16	2.24	0.21
NH_4NO_3, %,~1045 cm^{-1}	0.90	0.13	1.07	0.07	1.71	0.30
$Ca(NO_3)_2$, %,~1051cm^{-1}	1.80	0.27	0.48	0.06	0.85	0.15
$NaNO_3$, %, ~1067cm^{-1}	5.58	0.49	0.00	0.00	21.94	1.73
Na_2CO_3, %,~1080 cm^{-1}	0.00	0.00	0.00	0.00	0.00	0.00
$CaCO_3$, %, ~1086 cm^{-1}	0.90	0.13	0.00	0.00	1.39	0.24
Inorganic Dominant Complex, %	3.82	0.14	7.60	0.25	14.07	0.48
$NaNO_3$+$CaCO_3$	0.63	0.09	0.00	0.00	3.10	0.27
NH_4NO_3+$CaSO_4$	0.00	0.00	2.40	0.11	0.00	0.00
NH_4NO_3+Na_2SO_4	0.00	0.00	0.60	0.08	0.00	0.00
$Ca(NO_3)_2$+NaNO3	0.00	0.00	0.00	0.00	0.93	0.16
$Ca(NO_3)_2$+Na_2SO_4	0.00	0.00	0.00	0.00	2.31	0.21
$Ca(NO_3)_2$+$CaSO_4$	0.90	0.13	0.67	0.09	1.85	0.32
$Ca(NO_3)_2$+$CaCO_3$	0.00	0.00	0.00	0.00	2.31	0.21
$NaNO_3$+ $CaSO_4$	0.90	0.13	0.00	0.00	0.93	0.16
$NaNO_3$+ Other organics	0.00	0.00	0.00	0.00	1.78	0.16
NH_4NO_3+ Other organics	0.63	0.09	0.48	0.06	0.85	0.15
$Ca(NO_3)_2$+Other organics	0.76	0.11	1.43	0.19	0.00	0.00
NH_4NO_3+$CaSO_4$+other organics	0.00	0.00	0.60	0.08	0.00	0.00
$Ca(NO_3)_2$+$CaSO_4$+other organics	0.00	0.00	1.43	0.19	0.00	0.00
Soil/Soot Dominant Complex%	69.98	0.79	74.79	0.16	30.88	1.61
Soil/Soot	39.58	1.59	48.86	1.14	15.95	0.89
Soil/Soot+ NH_4NO_3	5.89	0.57	3.79	0.25	3.63	0.43
Soil/Soot+ $NaNO_3$	4.69	0.51	0.00	0.00	5.95	0.46
Soil/Soot+ $CaSO_4$	1.66	0.13	2.10	0.16	1.78	0.16
Soil/Soot+ $CaCO_3$	2.77	0.21	0.00	0.00	0.85	0.15
Soil/Soot+ $Ca(NO_3)_2$	1.39	0.11	3.81	0.50	0.00	0.00
Soil/Soot+ $CaCO_3$+$NaNO_3$	0.90	0.13	0.00	0.00	0.00	0.00
Soil/Soot+ $Ca(NO_3)_2$+$CaSO_4$	1.39	0.11	0.95	0.12	0.93	0.16
Soil/Soot+ $Ca(NO_3)_2$+$CaCO_3$	3.32	0.25	0.00	0.00	0.00	0.00
Soil/Soot+ NH_4NO_3+$CaSO_4$	1.53	0.12	4.24	0.20	0.00	0.00
Soil/Soot+ NH_4NO_3+$NaNO_3$	0.90	0.13	0.00	0.00	0.93	0.16
Soil/Soot+ NH_4NO_3+Na_2SO_4	0.00	0.00	1.19	0.16	0.00	0.00
Soil/Soot+ $Ca(NO_3)_2$+Other organics	0.76	0.11	5.43	0.58	0.00	0.00
Soil/Soot+ NH_4NO_3+Other organics	3.06	0.24	3.55	0.17	0.85	0.15
Soil/Soot+Other organics	2.14	0.20	0.60	0.08	0.00	0.00

VITA

Name: Lijun Zhou

Address: Department of Atmospheric Sciences, Texas A&M University, 3150 TAMU, College Station, TX, 77843-3150

Email Address: lljjzhou@neo.tamu.edu

Education: B.A., Applied Chemistry, Qingdao University at Qingdao, China, August 2002
M.S., Atmospheric Sciences, Peking University at Beijing, China, August 2006